# A Hybrid LCC-VSC HVDC Transmission System Supplying a Passive Load

by

Omar Kotb

A thesis

presented to the University of Ontario Institute of Technology

in fulfillment of the

thesis requirement for the degree of

(Master of Applied Science)

in

(Electrical and Computer Engineering)

Oshawa, Ontario, Canada, 2010

## AUTHOR'S DECLARATION

I hereby declare that I am the sole author of this thesis. This is a true copy of the thesis, including any required final revisions, as accepted by my examiners.

I understand that my thesis may be made electronically available to the public.

## Abstract

High Voltage Direct Current (HVDC) transmission systems continue to be an excellent asset in modern power systems, mainly for their ability to overcome the problems of AC transmission, such as the interconnection of asynchronous grids, stability of long transmission lines, and use of long cables for power transmission.

In the past 20 years, Voltage Source Converter (VSC)-HVDC transmission systems were developed and installed in many projects, thereby adding more operational benefits to DC transmission option, such as high controllability, ability to supply weak networks, and reduced converter reactive power demand. Nevertheless, VSC-HVDC transmission suffers from the disadvantages of high losses and cost.

In this research, a hybrid HVDC employing a Line Commutated Converter (LCC) as rectifier and a VSC as inverter is used to supply a passive network through a DC cable. The hybrid system is best suited for unidirectional power transmission scenarios, such as power transmission to islands and remote load centers, where the construction of new transmission lines is prohibitively expensive. Control modes for the rectifier and inverter are selected and implemented using Proportional Integral (PI) controllers. Special control schemes are developed for abnormal operating conditions such as starting at light load and recovering from AC network faults. The system performance under steady state and transient conditions is investigated by EMTP-RV simulations. The results show the feasibility of the hybrid system.

# Acknowledgements

قُلْ إِنَّ صَلاتِي وَنُسُكِي وَمَحْيَايَ وَمَمَاتِي لِلَّهِ رَبِّ الْعَالَمِينَ (١٦٢) لاَ شَرِيكَ لَهُ وَبِذَلِكَ أُمِرْتُ وَأَنَاْ أَوَّلُ الْمُسْلِمِينَ (١٦٣)

سورة الأنعام: ١٦٢-١٦٣

(162. Say: "Verily, my prayer, my sacrifice, my living, and my dying are for Allah, the Lord of all that exists.") (163. "He has no partner. And of this I have been commanded, and I am the first of the Muslims.") Quran 6: 162-163

I would like to begin by thanking Allah, Most Strong, All Almighty, for providing me the strength and perseverance required to achieve this work. I would like to express my deep gratitude to my supervisor, Dr. Vijay Sood, who has been supporting and encouraging me throughout the project. It would not have been possible for me to achieve this work without his crucial guidance. I would also like to thank my parents and my sister for their steadfast support and encouragement, their care and love has been indispensable at all times in my entire life. My special thanks to my aunt Fatma, who has been firmly supporting me since I came to Canada. I would like to thank my fiancée Abeer, the love of my life, for her wonderful support and inspiration. It is also unforgettable to thank my colleagues in the department for their continuous willingness to help and exchange knowledge. Finally, I would like to thank all professors and staff at UOIT for their tremendous effort that made it possible for me to conduct my research and make the utmost benefit from the time I spent in the program.

## Dedication

To my father, who taught me the meaning of endurance in the journey of life and diligence in work.

# Table of Contents

# List of Figures

# List of Tables

## List of Abbreviations and Symbols

| | |
|---|---|
| CB | Circuit Breaker |
| CSC | Current Source Converter |
| d-component | Direct axis-component |
| EMTP-RV | Electromagnetic Transients Program-Restructured Version |
| EPC | Equidistant Pulse Control |
| GTO Thyristor | Gate Turn Off Thyristor |
| HPD Filter | High Pass Damped Filter |
| HVAC | High Voltage Alternating Current |
| HVDC | High Voltage Direct Current |
| IGBT | Insulated Gate Bipolar Transistor |
| LCC | Line Commutated Converter |
| MI | Modulation Index |
| NPC | Neutral Point Clamping |
| pf | power factor |
| PI Control | Proportional Integral Control |
| PLL | Phase Locked Loop |
| pu | per-unit |
| PWM | Pulse Width Modulation |
| q-component | q-axis component |
| R-C | Resistance-Capacitance |
| RE | Receiving-End |

| | |
|---|---|
| RoW | Right of Way |
| SCC | Self Commutated Converter |
| SCL | Short Circuit Level |
| SCR | Short Circuit Ratio |
| SE | Sending-End |
| SHE PWM | Selective Harmonic Elimination PWM |
| SLD | Single Line Diagram |
| SPWM | Sinusoidal PWM |
| SVPWM | Space Vector PWM |
| STATCOM | Static Synchronous Compensator |
| THD | Total Harmonic Distortion |
| V-I | Voltage-current |
| VSC | Voltage Source Converter |
| VVVF | Variable Voltage Variable Frequency |
| XLPE | Cross-Linked Polyethylene |
| $\alpha$ | Firing angle |
| $\delta$ | Power angle |

# Chapter 1

# Introduction

## 1.1 Background

The power transmission to islands and remote load centers has been an ongoing concern for power system operators around the world. In many countries, power utilities have been required to deliver electrical power to islands from the power grid on the mainland. As environmental awareness continues to grow worldwide, the public opposition to the construction of new transmission lines and generating stations persists. The difficulty of granting approvals for the construction of new generation and transmission facilities has spurred power utilities to investigate alternative ways to increase the power transmission capability of existing lines, as well as to use submarine cables to transmit power to islands instead of building new generating stations.

Power transmission to islands by AC cables has been implemented with limited success. The capacitance of AC cables represents a problem since a charging current has to flow in the cable in addition to the load current. The flow of charging current has to be taken into account when determining the cable current rating. Thus, the cable is de-rated and the actual allowable current is significantly reduced below the rated cable current, causing inefficient utilization of the cable rating [1, 11]. Moreover, the charging current causes the total power losses in the cable to rise, thus the transmission efficiency is reduced. Although modern Cross-Linked Poly Ethylene (XLPE) insulated cables are characterized by a relatively low

capacitance as compared to oil filled cables, the practical limit for a XLPE insulated submarine AC cable is in range of 100 km. The maximum cable length quickly reduces as the voltage level is increased [1-4].

High Voltage DC (HVDC) transmission is a power transmission option that was considered since 1950s [41]. DC transmission represented a solution to the most onerous problems in power transmission, namely the exchange of power between asynchronous grids, the reduction of losses in bulk power, long distance transmission, and submarine power transmission through cables [5, 18, 24]. The use of long submarine DC cables is not prohibitive since the cable capacitance is charged only once when the cable is energized. Thus, it is possible to utilize the full rating of the cable since the charging current is negligibly small. The advantages of HVDC transmission over its HVAC counterpart have been described in [5, 6, 7, 8, 18, 24]. The suitability of HVDC for long submarine cable transmission has been described in [7, 12, 18]. The introduction of VSC-HVDC with its outstanding operational characteristics further bolstered the adoption of DC option for submarine power transmission. The ability to supply weak and passive networks, independent control of active and reactive power, and immunity against commutation failure are the most salient operational characteristics of VSC-HVDC [9-10]. VSC-HVDC is perfectly suited for use with cables since the voltage polarity remains the same for both directions of power flow over the tie [13-14]. The widespread use of VSC-HVDC is nevertheless restricted as a result of high converter losses, high converter device cost [20] and high dielectric stress on equipment insulation [9, 16]. The low rating of VSC devices also limits the VSC-HVDC system rating to the range of hundreds of megawatts. Maximum power and voltage ratings of up to 1200 MW and ±320 kV were reported in [15-17].

## 1.2 Review of Related Literature

The principle of operation of a 2-level VSC based HVDC employing sinusoidal Pulse Width Modulation (PWM) has been covered thoroughly in [4, 9, 13, 19, 29]. The 2-level VSC topology is preferred for its simple structure, control strategy [19], small DC capacitor size, and small footprint [21]. Multilevel VSC topologies employing Neutral Point Clamping (NPC) and Flying Capacitor Configuration were covered in [21, 22]. Multilevel converters allow using higher DC voltages and reducing the harmonic content of the output AC voltage, however their shortcomings are complex structure and control strategies, unequal device duties, and larger footprint [21, 22]. Research on the PWM techniques to reduce switching losses has been made in [23].

The modeling and control of VSC-HVDC in light of vector control theory have been covered in [25-29]. The outer loop PI controllers generate setpoints for the inner loop current controllers that are used to control the VSC [25, 27, 29]. There are different control objectives for the outer loop controllers, these include: DC voltage control, active power control, frequency control, AC voltage control, and reactive power control [25]. The active power balance is achieved by controlling DC voltage at one end and controlling active power at the other end [25, 28]. Static Synchronous Compensator (STATCOM) operation of each VSC at both ends of the DC link could be implemented for the purpose of reactive power compensation in the connected AC networks. STATCOM operation is possible even when the active power transferred is zero [28]. The use of vector control strategy allows independent control of either active and reactive power, or active power and AC voltage [25]. The control strategies for a VSC-HVDC system supplying a passive load were discussed in [30-34]. The adoption of AC voltage control for the converter station supplying a dead

network was emphasized in [30-32]. Hybrid HVDC systems were investigated in [35-38]. The suitability of the hybrid system in supplying weak and passive networks was emphasized in [36, 37]. The immunity of the hybrid system to the stability problems that are often encountered in conventional HVDC transmission is emphasized in [37]. In [36], the hybrid system was used to supply an active network, the control strategy adopted DC voltage control and DC current control for rectifier and inverter stations, respectively. In [37], mathematical modeling of the hybrid system was developed; the normal operation of the hybrid link was also validated by simulation results.

## 1.3 Summary

This chapter presents an overview of the role of HVDC transmission in supplying islands by subsea cables. The advantages of HVDC transmission over its AC counterpart are mentioned and explained. The advantages of VSC-HVDC transmission over its conventional counterpart are also enumerated. A review of related literature for technical papers on VSC-HVDC transmission control and operation is made. An overview of technical papers on the concept of hybrid HVDC transmission system is finally presented. It could be concluded that a hybrid HVDC transmission system would allow utilizing the benefits of VSC-HVDC at the receiving end network while having a conventional Line Commutated Converter (LCC) at the sending end. This helps reducing the cost and losses of the transmission system.

# Chapter 2

# HVDC Transmission

## 2.1 Introduction

HVDC transmission technology is used to transmit DC electrical power over DC transmission lines or cables. AC power is converted to DC power at a rectifier station at the sending-end of the DC link, and the DC power is converted back to AC power at the inverter station at the receiving-end of the DC link. HVAC transmission is characterized by major advantages, namely the ease of alteration of voltage levels by transformers and the feasibility of meshed grids due the availability of AC circuit breakers. For these reasons, HVAC was overwhelmingly adopted for power transmission. Nevertheless, HVDC transmission is characterized by a number of operational benefits to the interconnected power systems. The key advantages of HVDC transmission are [40, 42]:

- Capability to interconnect asynchronous grids: since AC power is converted to DC power, the DC link acts as a buffer zone that provides isolation between two systems. Therefore a DC link could interconnect two power systems having different frequencies or having the same frequency but being asynchronous. This advantage makes the HVDC transmission the only feasible option for interconnecting asynchronous AC systems.
- Elimination of technical limits of line length: the power flow over a DC line is fully controllable by system controls at the converter stations. Thus, no

stability constraints exist for a HVDC line and the maximum power flow is determined by the rating of converters and the thermal rating of conductors. This advantage makes the HVDC transmission an ideal option for bulk power transmission over long distances, since stability constraints often limit the maximum possible length of HVAC lines.

- Reduction of power losses: for large amounts of power (typically above 1000 MW) and long transmission distances (typically above 500 km), the power losses in HVDC line are less than those in a comparable HVAC line. This is due to the absence of reactive power flow over HVDC lines, unlike HVAC lines where the flow of a reactive component of current leads to an increase in the total losses in conductors. Slight improvements in transmission efficiency lead to significant savings in case of a bulk amount of power being transmitted, therefore the use of HVDC transmission is justified in case of bulk power transmission over a long distance.

HVDC converters were initially of the Line Commutated Converter (LCC) type. These converters rely on the connected AC network for the commutation process in the converters. The converters initially employed mercury arc rectifiers as switching devices. The first commissioned HVDC project, in 1954, was a cable link between the island of Gotland and the Swedish mainland. The system was rated at ±100 kV, 20 MW. The development in high power solid state switches allowed thyristors to replace mercury arc rectifiers in the converters. The first HVDC project that was fully based on thyristors was commissioned in 1972 at Eel River in NB, Canada. The highest rated HVDC system was

commissioned in stages from 1984-1987 in Brazil; the system is rated at ± 600 kV, 6300 MW [39]. Now, the next level of transmission is planned at ± 800 kV in China [41].

Despite its operational benefits, the conventional HVDC transmission suffers from a number of drawbacks caused mainly by the reliance of converter commutation on the connected network voltage. These drawbacks mainly include: large consumption of reactive power, inability to supply weak networks, and large harmonic filters requirement.

A novel technology for HVDC transmission based on self-commutated converters (SCCs) was introduced in the early 1990s. The technology employed Voltage Source Converters (VSC) topology instead of the Current Source Converters (CSC) topology that was adopted for LCC. The novel technology was made possible by the development of high power self commutated devices, namely IGBTs and GTO thyristors. The VSC originally came from motor drive applications, where a DC voltage is processed by ON/OFF controlled power switches to produce Variable Voltage, Variable Frequency (VVVF) AC voltage to control the motor speed. PWM control of VSC using high frequency switching (1-2 kHz) of converter valves produces an AC voltage whose dominant harmonics are equal to multiples of the switching frequency (in range of kHz). The elimination of higher order harmonics, in range of kHz, becomes less problematic as the size and rating of harmonic filters are reduced. Since a VSC is fully controlled, the converter has little or no requirements of reactive power compensation. Therefore, the space requirement for a VSC converter station is less than that for a comparable LCC converter station. This feature reduces the footprint of converter stations and leads to significant cost reductions.

## 2.2 Configurations of HVDC Transmission

The commonly used HVDC configurations are the monopolar, bipolar, and back-to-back configurations. A brief description of each configuration is given below.

### 2.2.1 Monopolar

The monopolar configuration uses one conductor between both converters while the return path is through ground or sea. It is used with relatively low power ratings and in contingency conditions with bipolar systems.

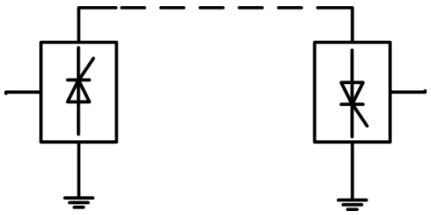

**Figure 2.1 Monopolar HVDC configuration**

### 2.2.2 Bipolar

The bipolar configuration is the most widely used one in HVDC transmission. Two converters are used at each end of the link and the midpoint between the converters is grounded. Thus, the upper converter operates with a positive DC voltage with respect to ground, while the lower converter operates with a negative DC voltage with respect to ground. Ground path is used by both converters and the DC currents flow in opposite directions in the ground. Therefore the net ground DC current is very small and it has little effect on the neighboring metallic structures.

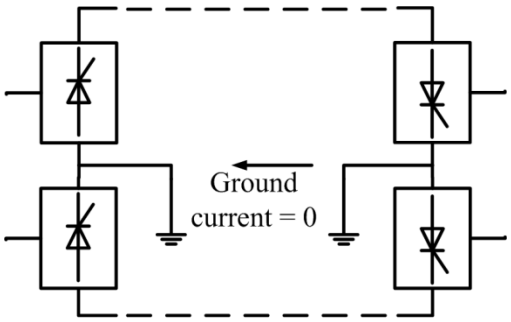


**Figure 2.2 Bipolar HVDC configuration**

### 2.2.3 Back-to-Back

Back to back configuration is used to interconnect two neighboring AC systems, with both rectifier and inverter located at one station. This configuration is mostly used to tie asynchronous systems.

## 2.3 Conventional HVDC Transmission

### 2.3.1 Converter Station

A Converter station is the most important element of a HVDC transmission system. A HVDC system includes at least two converter stations. The sending-end station operates in rectifier mode to perform AC/DC conversion, while the receiving-end station operates in inverter mode to perform DC/AC conversion. In addition to converters, a converter station also includes other equipment necessary for the control and protection of HVDC system. These mainly include: transformers, AC filters, DC filters, DC reactor, control and protection system, and converter cooling system. A brief description of the converter

station components is given below. The layout of a typical converter station is shown in Fig. 2.3.

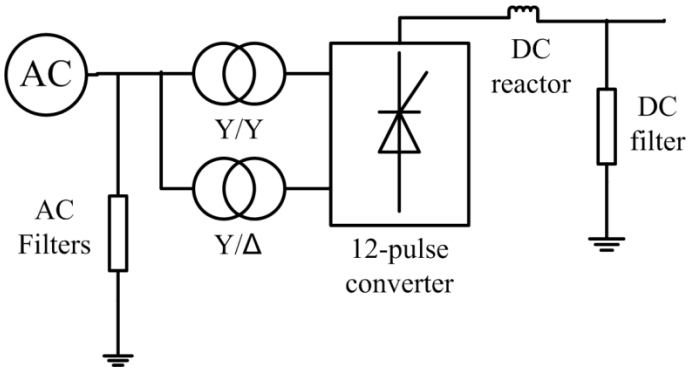


**Figure 2.3 Layout of converter station**

The components of the converter station are detailed as follows [40, 42, 45]:

- Converter

  A converter performs AC/DC conversion at the sending-end (rectifier) station and DC/AC conversion at the receiving-end (inverter) station. The basic building block of the converter is the 6-pulse thryistor bridge shown in Fig. 2.4. A converter is connected to the AC system by a transformer that alters the AC system voltage to a value suitable for the converter. A 12-pulse converter is built by connecting two six pulse bridges in series. A special transformer configuration is used for a 12-pulse converter, in which the upper and lower windings at the converter side are connected in Y and Δ connections, respectively. The converter side voltage of the lower transformer is displaced by $30^o$ from the voltage of the upper transformer. The use of a 12-pulse converter has the benefit of reducing the size and cost of harmonic filters by increasing the order of dominant harmonics.

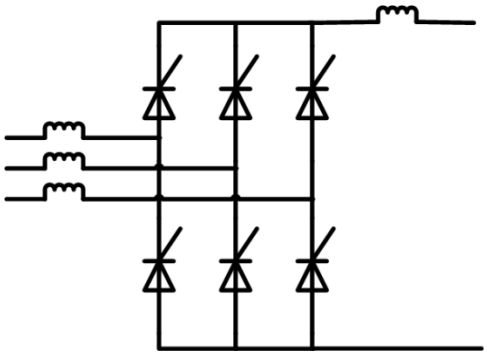

**Figure 2.4 6-pulse thyristor bridge**

- Converter Transformer

  Transformers are used to connect the converters to the AC system. They alter the AC voltage level to a value suitable for the power converter and the DC voltage rating. Transformers also contribute to the commutation reactance and provide isolation between the converters and the connected AC system. The converter transformer is represented by the series inductance in Fig. 2.4.

- AC Side Harmonic Filters

  The operation of the converter to perform AC/DC and DC/AC conversion generates harmonics whose frequencies depend on the converter configuration. The dominant current harmonics on the AC side of a 12-pulse converter are typically $11^{th}$, $13^{th}$, $23^{rd}$, and $25^{th}$ harmonics. AC filters are installed at the AC system side of the converter transformer, they are used to limit the magnitude of current harmonics and reduce the Total Harmonic Distortion (THD) to an acceptable value to the AC system.

The converters also consume reactive power which is supplied partly by the AC harmonic filters; the rest of the reactive power requirement could be supplied by capacitor banks.

- DC Side Filters

  The DC output voltage of the converter contains even harmonics of the order 6n. These harmonics need to be removed by means of harmonic filters on the DC side to avoid causing telephone interference, especially in case of overhead lines [18, 40]. DC filters are smaller in size than their AC counterparts. A typical DC filter is a High Pass Damped (HPD) filter tuned at a frequency equal to the number of pulse of the converter.

- DC Reactor

  A DC reactor is used at the DC side of the converter to smooth DC voltage ripples and reduce current transients during contingencies. The reactor also helps protecting the converter valves from voltage surges coming from the DC line [18].

### 2.3.2 Transmission Medium

The transmission medium could be an overhead line or cable. An overhead line is the option of choice in case of power transmission over long distances. The Right of Way (RoW) of a HVDC line is less than that of a HVAC line for same amount of power being transmitted, since a DC line has 2 conductors only while an AC line has a minimum of 3 conductors. The cost per unit length for a HVDC also tends to be lower than that of HVAC for distances above 500 km since DC transmission uses two conductors only.

Underground cables are used when it is not feasible to use overhead lines due to environmental or safety concerns.

## 2.4 VSC-HVDC Transmission

### 2.4.1 Self Commutated Converters

The VSC-HVDC transmission was originally developed from motor drives applications [4]. Modern day motor drives employ Self-Commutated Converters (SCCs) with fully controlled power electronic switches that are capable of high frequency switching. The principle of operation of SCCs is fundamentally different from that of LCC used in conventional HVDC. The key difference between both types of converters is the current commutation from one converter switch to another. Since converter switches in a SCC are fully controlled (i.e. ON/OFF controlled), the switch turn off is made by a control signal given to the switch, while another switch in a different limb is turned on by a control signal to carry on the current (and hence the name, self commutated converter) [45]. The principle of switch turn off is completely different in a LCC, where the switch (mostly thyristor) is turned off as its current drops below a certain value (known as the holding current) as a result of the device becoming reverse biased due to the change in source polarity (and hence the name, line commutated converter) [45]. As a result of its reliance on line commutation, conventional HVDC is only suitable for use in relatively strong networks with high Short Circuit Levels. An indication of network strength is given by the Short Circuit Ratio (SCR), which is the ratio of Short Circuit Level (SCL), in MVA, to the rated DC power, in MW. The use of conventional HVDC is not restrictive in networks with SCR greater than 3. For networks having a SCR between 2

and 3, the installation of additional reactive power compensation devices is necessary [42, 43]. In contrast to conventional HVDC, VSC-HVDC is fully controllable in terms of converter commutation. Thus it is possible to use VSCs in weak networks with low SCLs, and even in dead networks with zero SCLs [44].

The converter topology used in SCCs is the VSC, where the converter operation is based on the presence of a fixed input DC voltage that is processed by the converter switches to produce an AC voltage output. IGBTs and GTO thyristors are the most widely used devices in VSCs. The devices are connected in series to build a valve that is capable of withstanding the total voltage rating of the converter.

Various switching techniques are used to synthesize AC voltage in VSCs. The switching technique strongly affects both harmonics in the output AC voltage and switching losses of the converter. The objectives of switching technique development is to reduce harmonics in the output voltage (and hence reduce the size of harmonic filter), as well as to reduce the switching losses (and hence reduce the overall power losses).

### 2.4.2 PWM Techniques

PWM is the most widely adopted VSC switching technique. The method employs, in its basic form, two waveforms to generate the driving signals of converter switches. The first is the reference wave which has the fundamental frequency of the voltage to be generated, and the second is the carrier wave, which has a higher frequency that is typically within 1-2 kHz. Both waveforms are introduced to a comparator that switches its output between high and low values, depending on the instantaneous value of both waveforms. A high comparator output activates the upper valve in a limb, while a low

output activates the lower valve in the same limb. Thus, the AC output voltage of each phase varies between positive and negative DC values. The modulation index (MI) is defined as the ratio of the magnitude of the reference wave to the magnitude of the carrier wave.

Different types of PWM include Sinusoidal PWM (SPWM), Space Vector PWM (SVPWM), Optimal PWM, and Selective Harmonic Elimination (SHE) PWM. The selection of PWM technique mainly depends on the type of application. SPWM is widely used for VSC-HVDC for its simplicity and ease of implementation.

### 2.4.3 Components of VSC-HVDC Transmission

- Converter station

  The converter station includes the VSC along with transformers, AC filters, DC capacitors, and phase reactors. A description of each of these elements is given below.

  *(a) Converter*

  The converter is comprised of fully controlled electronic valves connected in a bridge configuration. The 2-level VSC configuration is widely used for its simple design, other configurations include multilevel diode clamped and flying capacitor converters. Multilevel converters have the advantages of lower harmonic content and switching frequency, and consequently lower switching losses. However they are characterized by an increased complexity in circuit construction and control method, and consequently they are more

costly than 2-level VSCs. The 2-level and 3-level VSC topologies are shown in Figs 2.5 and 2.6, respectively.

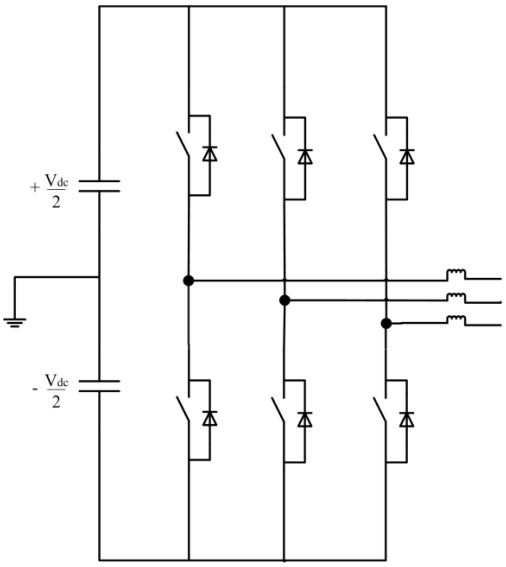


**Figure 2.5 2-level VSC**

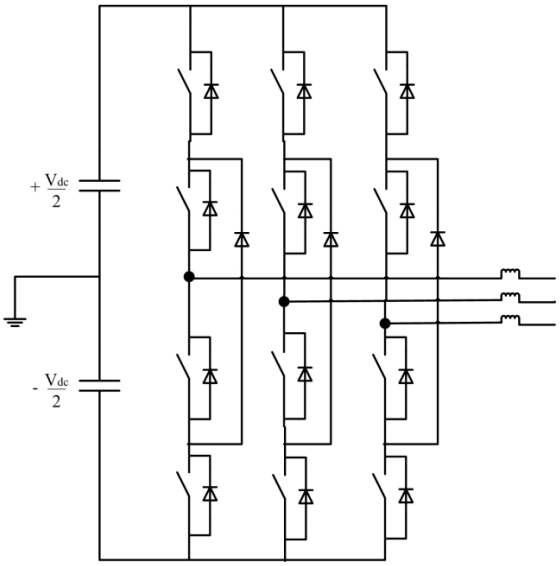


**Figure 2.6 3-level diode clamped VSC**

*(b) Transformers*

Transformers are used to adapt the AC system voltage to a value suitable for the VSCs. Transformer reactance also contributes to the total reactance between the converter and AC system, and therefore, together they help to control the power exchanged between the converter and the AC system.

*(c) AC Filters*

A VSC generates an AC voltage waveform that varies between two values of DC voltage. The voltage waveform includes a fundamental component as well as higher order harmonics whose frequencies

depend on the value of switching frequency. The dominant harmonic frequencies are usually multiples of $f_s \pm f$, where $f_s$ and f are the switching frequency and fundamental frequency respectively. Passive filters are installed at the AC bus to remove higher order harmonics and reduce the THD.

*(d) DC Capacitors*

The role of DC capacitors is to maintain a constant DC voltage input to the VSC and provide the voltage support for converter dynamics. DC capacitors also help in smoothing the DC voltage ripples [32].

- Transmission Medium

Both overhead lines and cables could be used with VSC-HVDC. However, it is preferred to use cables. The reason for preference of cables is the topology of VSC that does not include a means to interrupt a DC fault current that may occur. When a DC fault takes place, the converter bridge will feed the fault from the AC network via anti parallel diodes; the absence of a DC reactor will cause very high currents to flow towards the fault. Since DC CBs are uneconomical to be used, the fault could only be cleared by tripping the AC CB that feeds the converter itself. To avoid such a situation, cables are used with VSC-HVDC since they significantly reduce the risk of a DC fault.

# 2.5 VSC Control

## 2.5.1 VSC Modeling

A VSC produces a PWM voltage that contains a fundamental frequency component in addition to harmonics. The magnitude of the fundamental frequency voltage of the converter is controlled by the Modulation Index (MI) which is defined as:

$$MI = \frac{A_{reference}}{A_{carrier}} \tag{2.1}$$

Where $A_{reference}$ is the amplitude of the reference waveform, and $A_{carrier}$ is the amplitude of the carrier waveform.

The VSC is modeled as a voltage source with variable magnitude and phase. The vector diagram of converter voltage and system voltage is shown in Fig. 2.7. $V_{con}$ refers to the rms value of the fundamental component of converter voltage, while $V_s$ refers to the RMS value of system voltage. The active power flow between a VSC and an AC system is determined by the value of angle δ, while the reactive power flow is determined by the value of $V_{con}$. In the vector diagram in Fig. 2.7, the VSC operates in inverter mode and the active power flows from the VSC to the AC system. Since the magnitude of converter voltage is greater than that of the system voltage, the reactive power flow is from the VSC to the AC system. The operating modes of VSC are shown in Fig. 2.8.

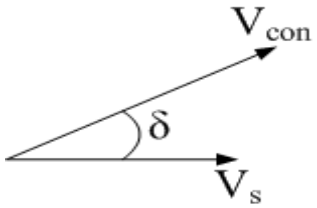


**Figure 2.7 Vector diagram of converter voltage ($V_{con}$) and system voltage ($V_s$)**

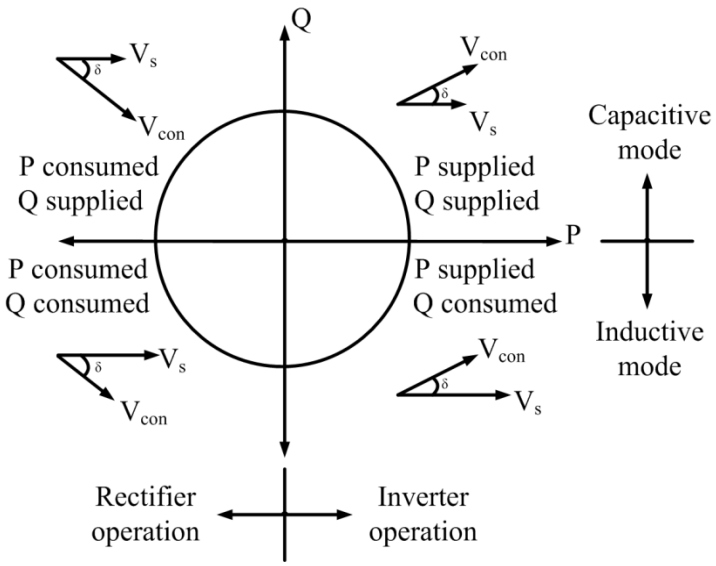


**Figure 2.8 Operating modes of VSC**

Considering the VSC in Fig. 2.9, the voltage equation could be written as follows:

$$V_{con}^{abc} = V_S^{abc} + i^{abc}R_S + L_S\frac{di^{abc}}{dt} \tag{2.2}$$

The active and reactive power exchanged between the VSC and the AC system could be expressed as follows (neglecting the power losses in $R_s$):

$$P = \frac{|Vcon|\times|Vs|}{Xs}\sin\delta \tag{2.3}$$

$$Q = \frac{|Vcon|\times|Vs|}{Xs}\cos\delta - \frac{|Vs|^2}{Xs} \tag{2.4}$$

Where P is the active power, Q is the reactive power, and $X_s$ is the transfer reactance between the converter and the system. From the above equations, it shows that real and reactive powers are controlled by $V_{con}$, $V_S$, and δ.

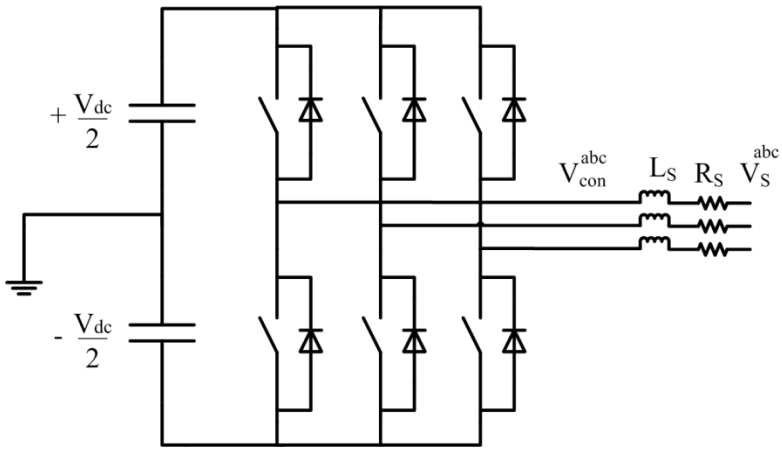


**Figure 2.9 VSC connected to an AC system**

## 2.5.2 VSC Control Strategies

The control objectives of a VSC mainly depend on the AC system to which the VSC is connected. The controlled parameters are regulated using two degrees of freedom (controlling parameters) at each converter station; the first is the magnitude of converter voltage ($V_{con}$) while the second is the phase angle ($\delta$) between converter voltage and AC system voltage. The classification of control objectives at converter stations is given as follows [32]:

- Supply to a passive network without local generation

  **Sending-end:** DC voltage control and AC voltage control

  **Receiving-end:** AC voltage control and frequency control

- Interconnection of two or more active networks

  **Sending-end:** DC voltage control and AC voltage control

  **Receiving-end:** Real power control and AC voltage control

Direct control of VSC directly regulates the controlling parameters to achieve the control objectives. The concept of direct control is shown in Fig. 2.10. The figure shows both MI and phase angle δ being regulated to achieve control of AC voltage and active power respectively.

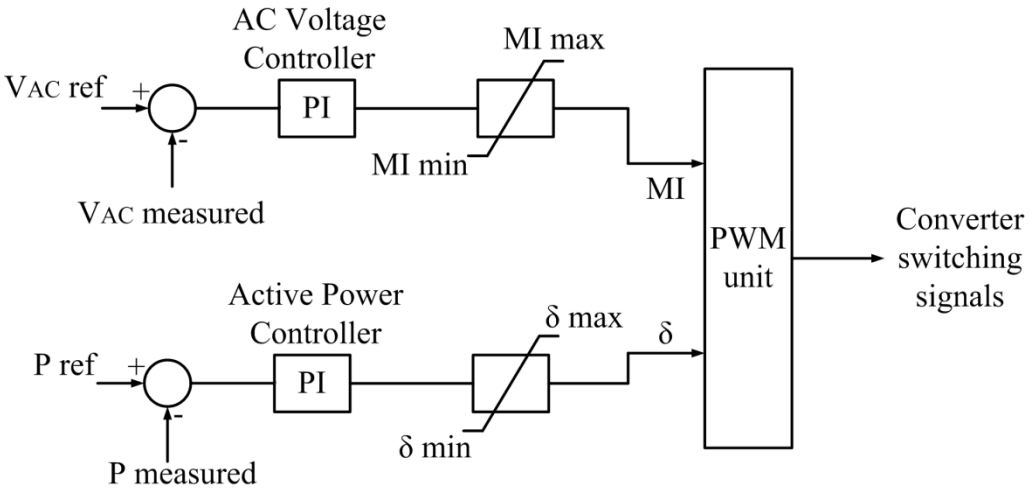


**Figure 2.10 Direct control strategy [47]**

Vector control adopts vector control theory to regulate direct (d) and quadrature (q) current components independently. The block diagram of vector control is shown in Fig. 2.11. The currents and voltages are converted from three phase frame to the d-q frame. Upon conversion from abc frame to d-q frame, the reference axis of d or q component is synchronized with phase A of three-phase voltage of the connected AC system by means of a Phase Locked Loop (PLL). Thus, the system voltage is locked to the d or q reference axis and its full value is either $V_{sd}$ or $V_{sq}$. The phase angle between the converter voltage and the system voltage is δ, which is calculated from the outputs of inner loop controllers in Fig. 2.11 according to equation (2.5). On the other hand, the modulation index is also calculated from the outputs of inner loop controllers according to equation (2.6).

$$\delta = \tan^{-1}\frac{V_{cq}}{V_{cd}} \tag{2.5}$$

$$MI = \sqrt{\left(V_{cd}^2 + V_{cq}^2\right)} \tag{2.6}$$

The controllers' configuration in Fig. 2.11 assumes that the d-axis is synchronized to the system voltage, and therefore the outer loop controller, supplying $I_{d\ ref}$, could be used to regulate the DC voltage or active power. On the other hand, the outer loop controller, supplying $I_{q\ ref}$, could be used to regulate the AC voltage or reactive power. The choice of controlled variable of the outer loop controller depends on the operating mode of the VSC as rectifier or inverter, as well as the nature of connected AC system and the required control objectives to be achieved.

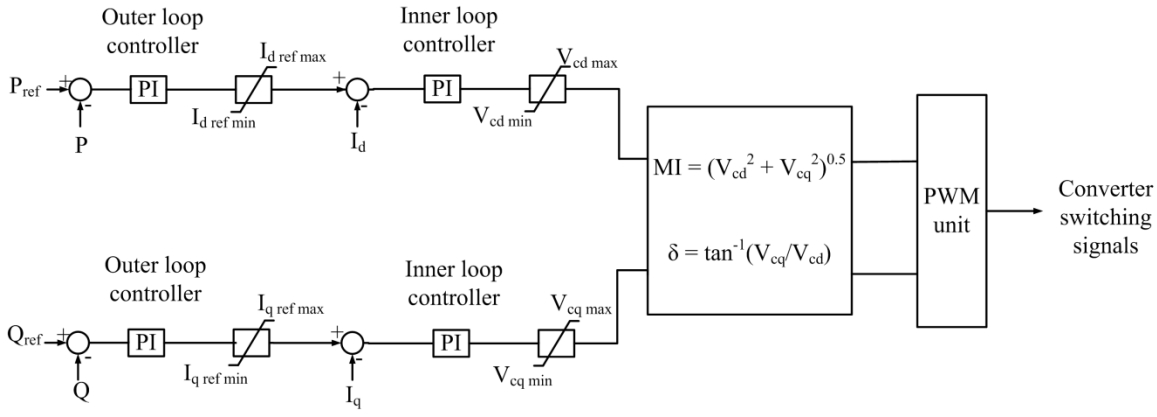


**Figure 2.11: Vector control of VSC**

## 2.6 Summary

This chapter presented a detailed description of the components of conventional HVDC transmission and VSC-HVDC transmission. The PWM switching technique of VSC was presented and its various types were enumerated. The modeling of VSC and its

control strategies were also discussed. The operating modes of VSC, as a rectifier and as an inverter, were presented and discussed. It could be concluded that the VSC's ability for independent control of output voltage magnitude and phase angle is an outstanding feature that enables a wide number of control objectives to be achieved in the connected AC network.

# Chapter 3

# Objectives

The VSC-HVDC transmission is characterized by its independent control of active and reactive power, ability to supply weak and passive networks, reduction of harmonic filters size, and suitability for use with DC cables since voltage polarity is always the same. However, serious drawbacks such as high power losses, high dielectric stress on equipment insulation, and low device rating restrict the widespread use of VSC-HVDC transmission. A DC tie with identical VSCs at both ends allows bidirectional power flow. In many cases, however, the power flow in the DC tie is predominantly unidirectional. Such cases include power transmission to islands and remote isolated load centers, where the receiving network is passive and lacks any form of local generation. In this research, a hybrid LCC-VSC HVDC transmission system supplying a passive load is investigated. The system consists of a LCC connected to the sending-end AC network, and a VSC connected to the receiving-end network. The power flow in the system is always unidirectional. The power is exported from the sending-end AC network via DC tie to the receiving-end passive network. The proposed system is best suited for power transmission to islands and remote load centers, since the receiving network is usually weak or even passive.

*Chapter 3 Objectives*

The main objectives of this thesis are the following:

- To develop a model for the hybrid HVDC transmission system supplying a passive load in EMTP-RV simulation environment
- To select the appropriate control modes for rectifier and inverter terminals in the hybrid system, in such a way that guarantees the proper operation of the system under steady state and transient conditions
- To develop special control schemes that cope with abnormal and transient conditions such as starting at light load and AC network faults
- To investigate and study the performance of the hybrid system with the developed control schemes under steady state and transient conditions using EMTP-RV simulations

# Chapter 4

# Methodology

## 4.1 Introduction

The implementation of a hybrid HVDC transmission system supplying a passive load was tested in EMTP-RV simulation environment. The EMTP-RV software is a computer program for the simulation of electromagnetic, electromechanical, and control system transients in multiphase electric power systems [46]. The program has readily available blocks for the system components such as converters, transformers, filter banks, and other circuit elements. The model building was started by considering each system terminal separately, and then both terminals were combined together to form the complete system.

The first terminal that was developed in the hybrid system was the inverter (receiving-end) terminal. A passive load was connected to the inverter model that was fed by a DC voltage source. The AC output voltage of the inverter was regulated by a PI controller. A block diagram of this stage of simulation work is shown in Fig. 4.1.

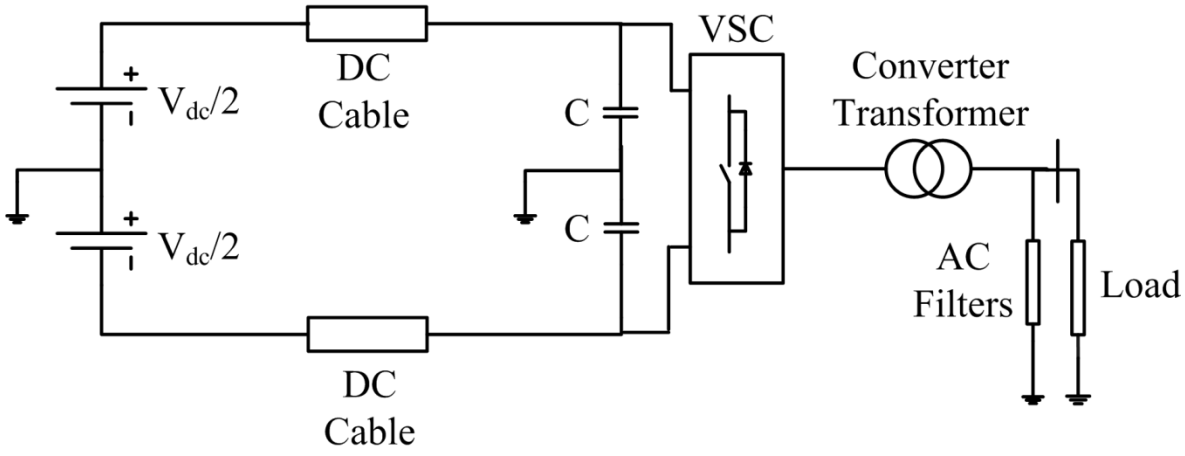


**Figure 4.1 Preliminary inverter terminal circuit**

The rectifier terminal was developed after the completion of inverter terminal build up. The preliminary rectifier model consists of a 12-pulse rectifier fed by an AC 3-phase source through impedance, which represents the sending-end network. The DC terminal of the rectifier was connected to a DC voltage source which represents the receiving-end terminal. The DC voltage of the rectifier was also regulated by a PI controller. The block diagram of this preliminary rectifier terminal circuit is shown in Fig. 4.2.

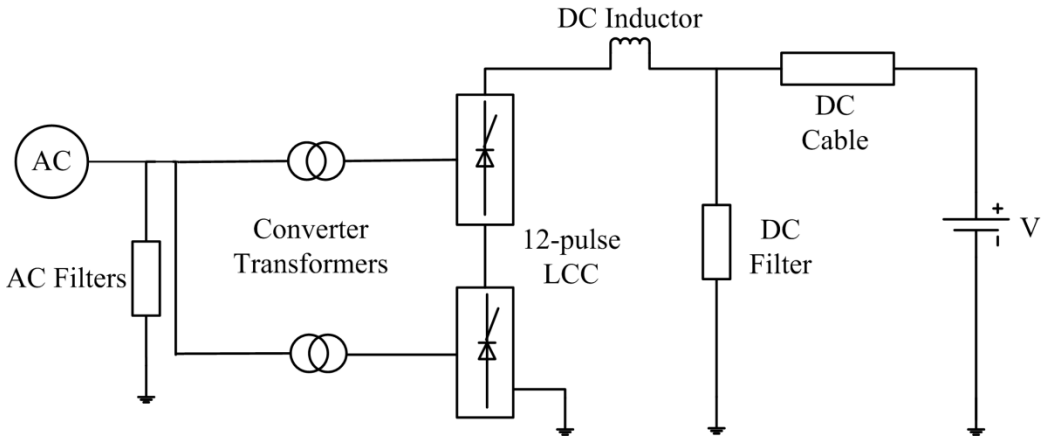


**Figure 4.2 Preliminary rectifier terminal circuit**

Each terminal of the system was first handled separately from the other. In the inverter terminal, the work focused on the regulation of load voltage, investigation on the effects of load change and load shedding, and the system response in case of faults on the AC side of the inverter. The work on the rectifier terminal focused on the regulation of DC voltage. The block diagram of the system in EMTP-RV is shown in Fig. 4.3.

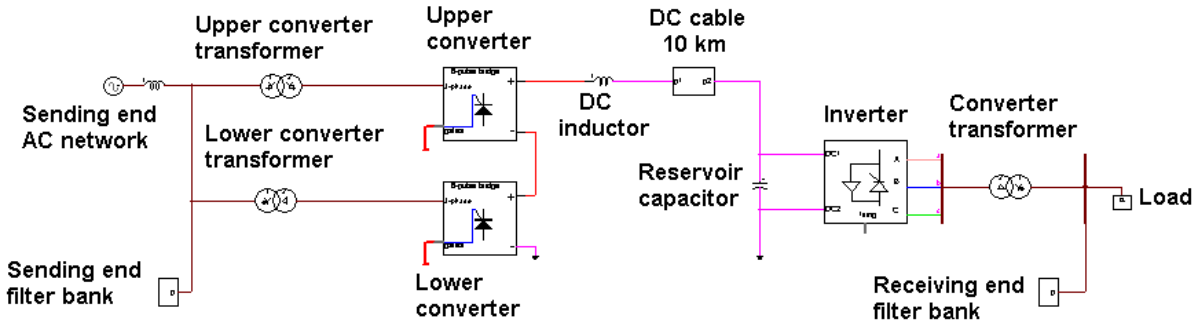


**Figure 4.3 Combined system (rectifier, inverter and DC cable) in EMTP-RV**

## 4.2 Modeling of Rectifier

### 4.2.1 Power Circuit

The rectifier terminal is a 12-pulse thryistor based converter. The converter is connected to the AC network through two converter transformers. The upper transformer has a Y/Y connection and the converter side voltage is in phase with the high voltage side. The lower transformer has a Y/Δ connection and the converter side voltage lags the high voltage side by $30^{o}$. The converter transformer steps down the voltage level of the AC system to a lower level that is suitable for the converter and also provides effective isolation between the

network side and the converter. The block diagram of the rectifier connection to the AC network is shown in Fig. 4.4.

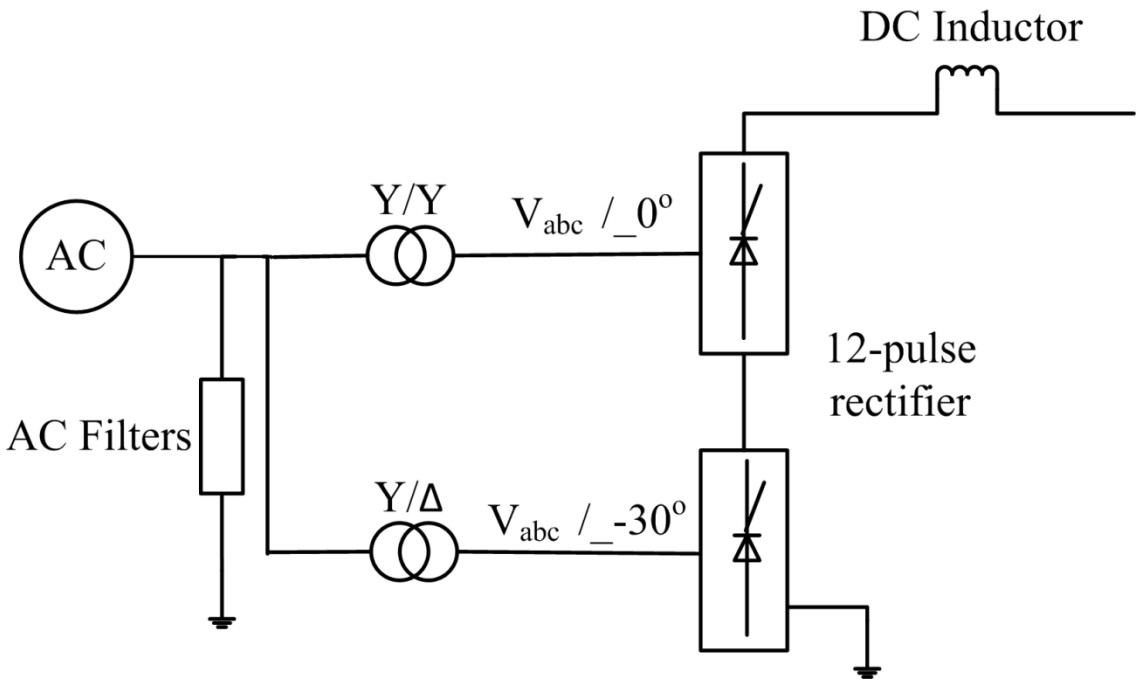


**Figure 4.4: Rectifier connection to the AC network**

The 12-pulse rectifier consists of two 6-pulse rectifier bridges connected in series. The bridges are fed from the Y/Y/Δ transformer that introduces a phase shift of 30° between the upper converter and lower converter voltages. Since the basic rectifier building block in EMTP-RV is the 6-pulse bridge, the 12-pulse rectifier was implemented in EMTP-RV by connecting two 6-pulse bridges in series.

The block diagram of the rectifier connection to the AC network is shown in Fig. 4.5.

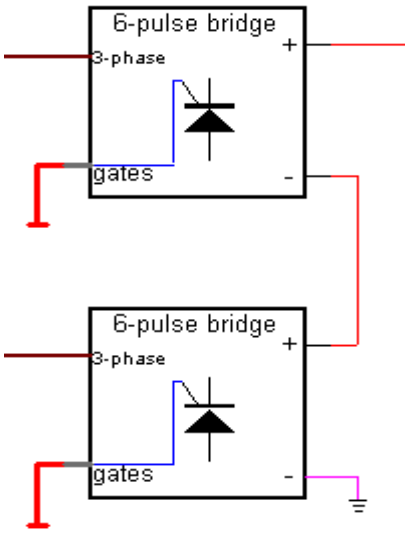


**Figure 4.5: 12-pulse rectifier in EMTP-RV**

### 4.2.2 Control Circuit

Each 6-pulse bridge receives the firing signals from a 6-pulse firing unit. Firing units are available in EMTP-RV for both 6-pulse and 12-pulse bridges. The firing units use the Equidistant Pulse Control (EPC) principle [43]. The firing pulse width is 1 ms which is split into two pulses by means of pulse doubling technique. Pulse doubling is used in order to ensure thyristor turn-on. The firing delay is calculated with respect to reference phase voltage signals that are fed to the firing unit through Phase Locked Loops (PLLs) [43]. The PLL synchronizes the firing pulses with respect to the fundamental component in the voltage waveform and therefore possible errors in zero crossing detection, due to harmonic content in the voltage waveform, are avoided. The block diagram of the rectifier control system in EMTP-RV is shown in Fig. 4.6.

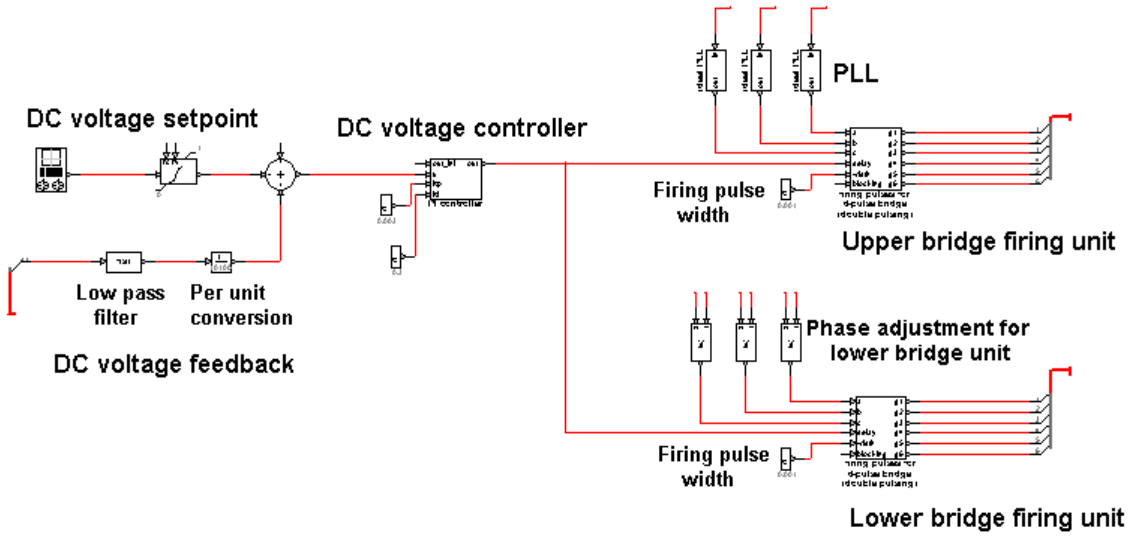


**Figure 4.6 Rectifier control system in EMTP-RV**

The DC voltage setpoint was fixed at 10.1 kV, which was taken as the base value in the rectifier control system. The measured value of DC voltage is fed back and divided by the base DC voltage value to be converted to pu value. The selection of controller gains was based on trial and error method with the objective of reducing the magnitude of DC overvoltage below 1.2 pu, and achieving a settling time for the system within 0.1-0.2 s. Thus, a series of simulation runs were conducted in order to optimize the controller gains by observing the system response. This resulted in selecting a proportional gain of 0.003 and an integral gain was set at 0.3.

## 4.3 Modeling of Inverter

### 4.3.1 Power Circuit

The receiving-end consists of the inverter, converter transformer, and load. The inverter is a 2-level VSC. The converter's fully controlled power devices were modeled in EMTP-RV

by controlled switches. A controlled switch in EMTP-RV is switched on or off upon the activation or de-activation of a control signal. R-C snubber circuits were used in parallel with the controlled switches.

The converter transformer connects the inverter to the load bus. This transformer steps up the converter output voltage to the voltage level of the load and provides isolation between the inverter and load sides. The voltage rating of the transformer on the inverter side was selected so as to guarantee that the insulation level could withstand the output voltage of the inverter. In a practical situation, however, a special design of the transformer is needed to avoid the breakdown of the insulation as a result of voltage stresses caused by fast converter switching.

### 4.3.2 Control Circuit

The inverter control circuit consisted of the following components:

- AC voltage controller
- PWM unit

The AC voltage controller is of a fixed gain PI type. The controller gains were selected based on trial and error method, with the objective of reducing the magnitude of AC overvoltage below 1.1 pu, and achieving a fast system starting, with settling time of 0.1-0.2 s. The value of the proportional gain was set at 0.45 while the value of the integral gain was set at 60. The AC voltage setpoint was set to 1 pu, which corresponds to 33 kV (line voltage) at the load bus. The three-phase voltage measurement signal was converted to pu value by dividing it by the base voltage first which was, in this case, the peak value of phase voltage. The pu normalized signal was then introduced to a maximum value selector block, which

acts similar to an uncontrolled rectifier by converting the three-phase voltage to a DC voltage. The rectified voltage signal is then introduced to a low-pass filter for the purpose of smoothing the output voltage and reducing its ripples. The block diagram of the voltage signal processing is shown in Fig. 4.7. The filter output is finally compared to the AC voltage setpoint and the error is processed through the AC voltage controller, whose output represents the modulation index. The feedback voltage signal and the outputs of signal processing stages are shown in Fig. 4.8. The block diagram of the inverter control system, including the PWM generator, is shown in Fig. 4.9.

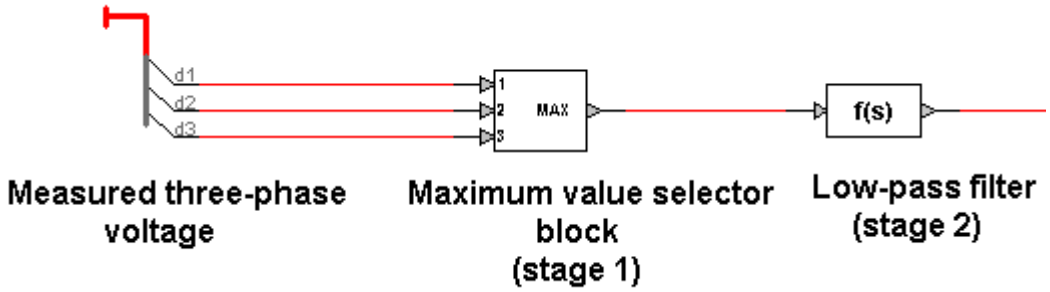


**Figure 4.7 Signal processing of measured voltage**

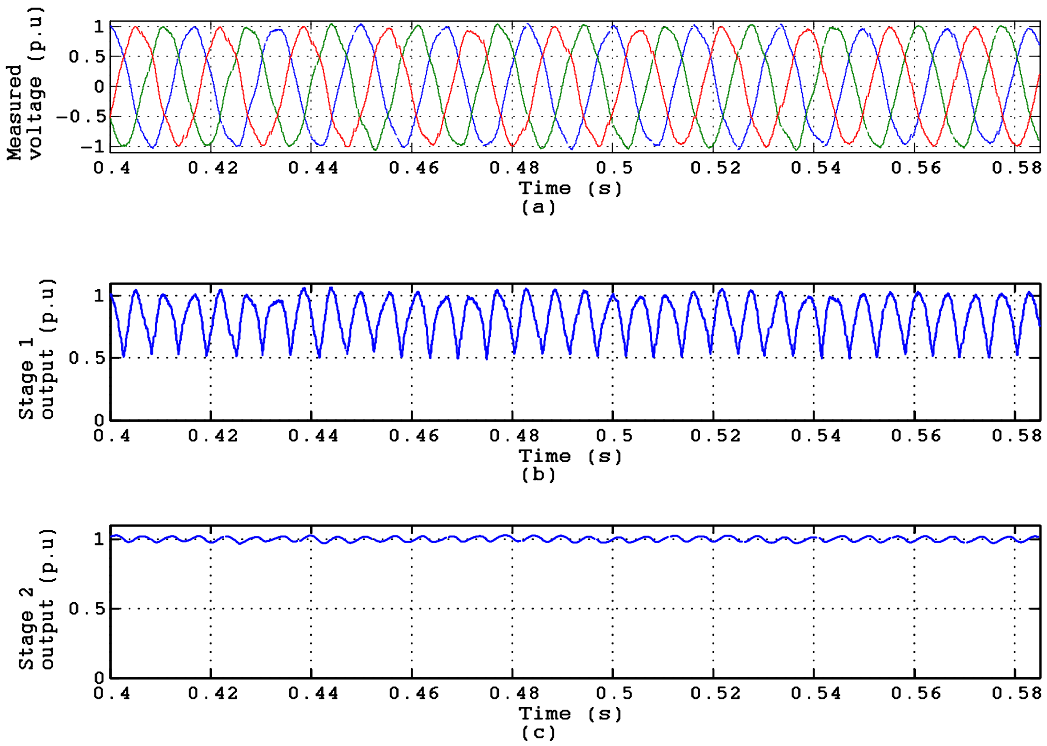


**Figure 4.8 Measured voltage and outputs of signal processing stages**

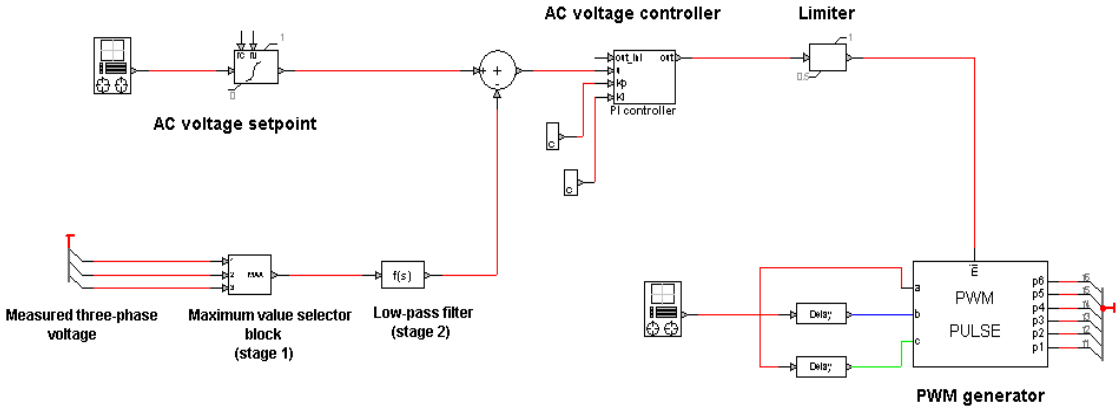


**Figure 4.9 Inverter control system in EMTP-RV**

The AC voltage controller stage was followed by the PWM generation stage, which has the function of generating the driving signals to the VSC switches. The PWM generator block is readily available in EMTP-RV. The carrier frequency was set to 1.5 kHz. The selection of carrier frequency is a compromise between high switching losses and adequate higher quality waveform generation. Bipolar switching technique was used in order to prevent the simultaneous operation of two switches on the same limb. The generation of fundamental frequency reference signals for PWM was made using signal generators. The generation of the carrier signal was made using a combination of a signal generator and an integrator. The block diagram of PWM generator is shown in Fig. 4.10. The waveforms of carrier and reference, and driving signals to converter valves of phase A are shown in Fig. 4.11.

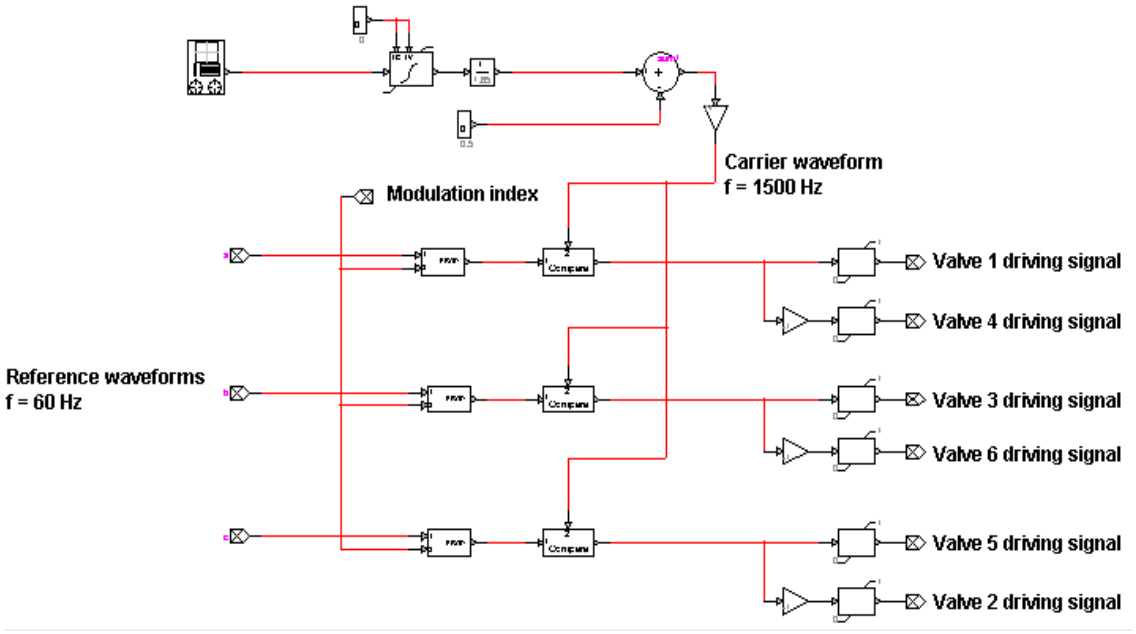


**Figure 4.10 PWM generator in EMTP-RV**

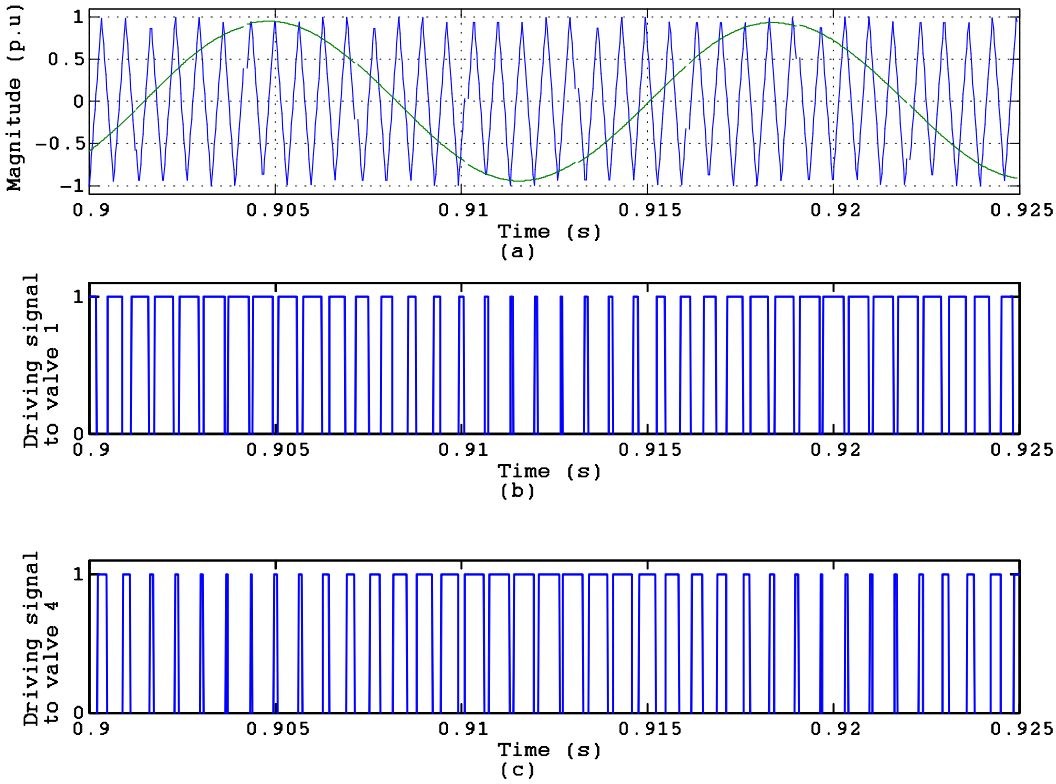


**Figure 4.11 Carrier and reference waveforms and driving signals to converter valves**

## 4.4 Modeling of DC Cable

The DC cable was modeled as a series of T-sections with resistance (R), inductance (L), and capacitance (C) components. The cable model has 4 T-sections; each series arm in a section consists of R-L elements. The value of R is 0.54 Ω and the value of L is 2.072 mH. The value of capacitance per section is 2 μF. The cable model in EMTP-RV is shown in Fig. 4.12.

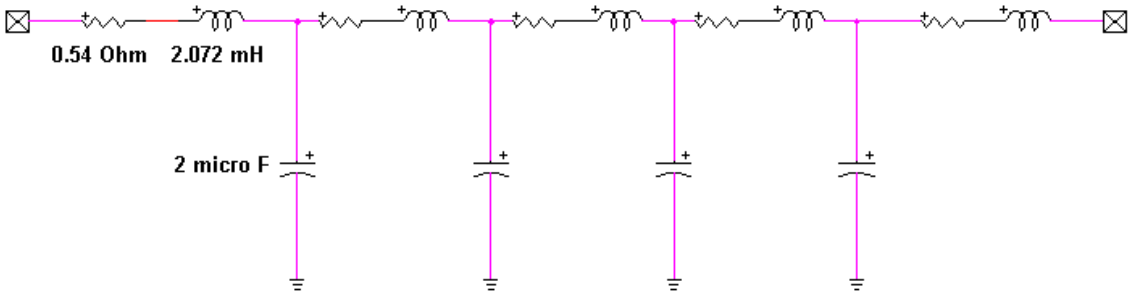


**Figure 4.12 DC cable model in EMTP-RV**

## 4.5 Modeling of Load

The load was modeled as fixed-impedance R-L branches. The receiving end network load was set at 2.4 MVA, 0.8 pf lagging. The load was split into 10 portions that are switched as required. The use of switched branches for load modeling was intended to replicate the situations of load changes. The block diagram of load model in EMTP-RV is shown in Fig. 4.13.

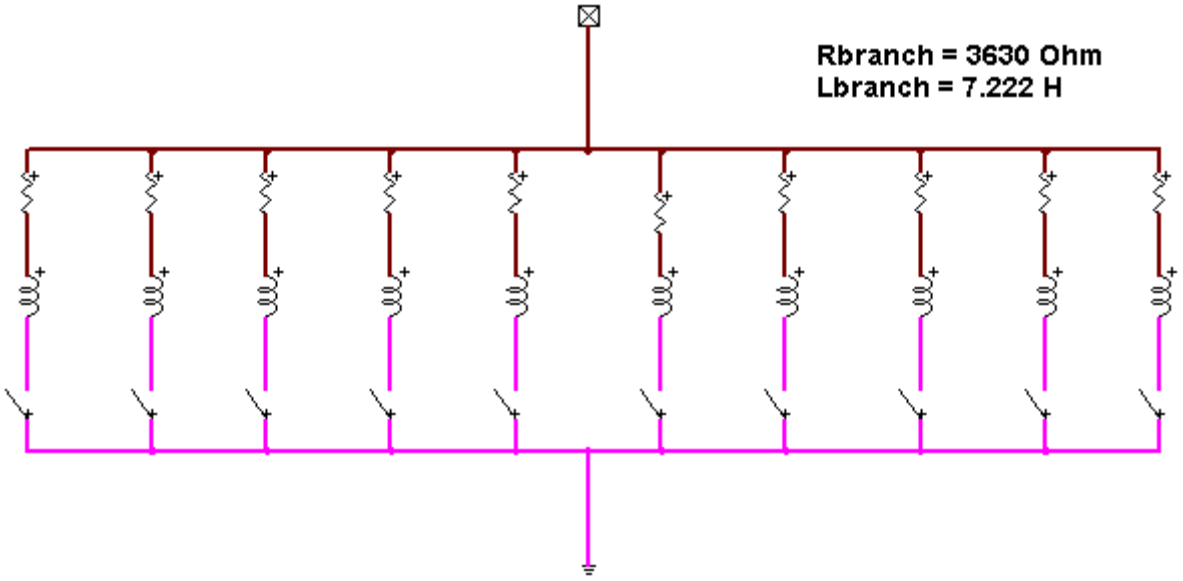


**Figure 4.13 Load model in EMTP-RV**

## 4.6 Summary

This chapter presented the modeling of hybrid HVDC system components in EMTP-RV. The implementation of system components in the simulation tool was presented. A description of the power and control circuits was made for the rectifier and inverter terminals. The implementation of signal processing in control circuits was also developed and presented. Finally, the models of DC cable and receiving-end passive load were presented.

# Chapter 5

# Test System

## 5.1 Introduction

The 2-terminal hybrid HVDC system consists of rectifier and inverter stations at the Sending-end (SE) and Receiving-end (RE) of the DC link respectively. The rectifier is a 12-pulse thyristor based LCC, while the inverter is a 2-level VSC. The Single Line Diagram (SLD) of the two-terminal system is shown in Fig. 5.1.

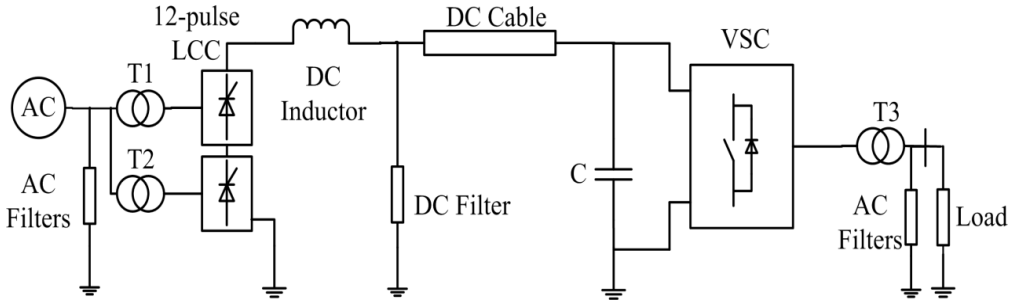


**Figure 5.1 SLD of two-terminal hybrid HVDC system**

The system was used to supply the passive network at the RE of the DC link. A 33 kV, 2.4 MVA, 0.8 p.f. lagging load was connected to the RE network. The system specifications are given in the Table 5.1.

**Table 5.1 Two-terminal hybrid system specifications**

| | |
|---|---|
| SE AC network | Rated voltage: 33 kV, SCL: 500 MVA |
| SE AC filters | Tuned filters: $11^{th}$ and $13^{th}$ harmonic filters, 0.45 MVAR each<br>HPD filter: $12^{th}$ harmonic, 0.15 MVAR |
| Converter transformers $T_1$ and $T_2$ | 33/4.5 kV, 3 MVA |
| Rectifier | 12-pulse LCC rated at 6 MW |
| DC inductor | 250 mH, 300 A |
| DC filter | HPD filter: $12^{th}$ harmonic, 0.45 MVAR |
| DC cable | Rated voltage: 12 kV, operating voltage: 10 kV, length:10 km |
| Reservoir capacitor | 100 μF, 12 kV |
| VSC | 2-level topology, 3 MVA |
| Converter transformer $T_3$ | 7.1/51 kV, 5 MVA |
| RE AC filters | HPD filter: $25^{th}$ harmonic, 0.5 MVAR<br>Capacitor bank: 0.6 MVAR |
| Load | 33 kV, 2.4 MVA, 0.8 p.f. lagging |

The V-I characteristics of the DC system are presented in Table 5.2. It is worth mentioning that these values correspond to the normal operating conditions, in which the system is operated in closed loop control mode. For system loads less than 0.4 pu, the system is switched to open loop control mode as explained in section 5.3.1. The base value for the system load is the rated load power of 1.92 MW.

**Table 5.2 V-I characteristics of the DC system**

| | | | | | | | |
|---|---|---|---|---|---|---|---|
| DC voltage (kV) | 9.5 | 9.5 | 9.6 | 9.7 | 9.85 | 10 | 10.1 |
| DC current (A) | 280 | 260 | 240 | 220 | 200 | 185 | 165 |
| System load (pu) | 1 | 0.9 | 0.8 | 0.7 | 0.6 | 0.5 | 0.4 |

## 5.2 Control System

The control strategy adopted is DC voltage control at the rectifier station and AC voltage control at the inverter station. The reason for this selection is to create a fixed voltage, fixed frequency supply for the passive network at the RE, while the DC link voltage is regulated by means of firing angle control at the rectifier station. The controllers used were of PI type as they are capable of eliminating the steady state error and achieving a satisfactory transient performance.

### 5.2.1 Rectifier Control System

The block diagram of the rectifier control system is shown in Fig. 5.2. As DC voltage control was adopted, the controlled parameter was the DC voltage while the controlling parameter was the firing angle of the rectifier bridge. In order to guarantee the existence of

sufficient forward voltage across the thyristor valve at the instant of firing, the the minimum firing angle was set to $5^o$, which is a typical standard practice in the design of rectifier controller. Although the system operation involves the converter being operated as a rectifier only, the maximum limit of the firing angle was set to $120^o$. This was intended to allow the firing angle increase during transients upon the DC voltage setpoint reduction, as explained in section 5.3.2. The voltage level of transformers $T_1$ and $T_2$ was selected in such a way to obtain a steady state firing angle of 15-$20^o$ at full load; this was intended to avoid excessive reactive power consumption by the rectifier.

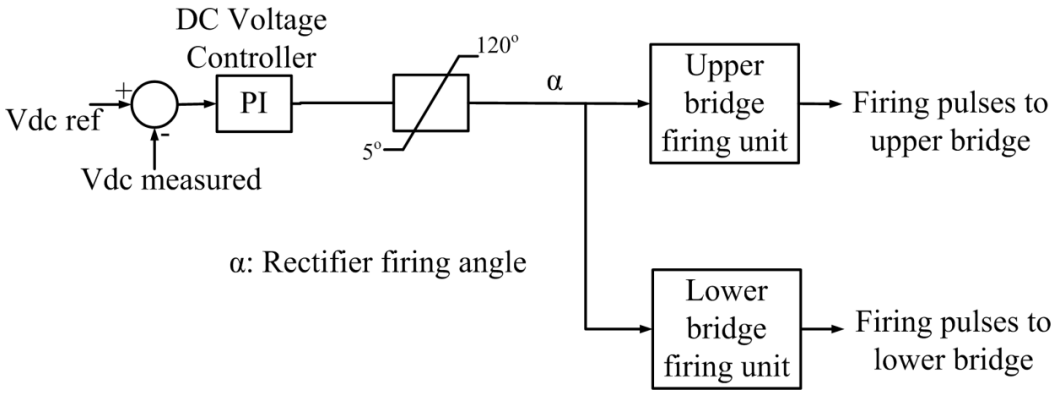


**Figure 5.2 Rectifier control system**

The inputs of bridge firing unit are: synchronizing reference signals, firing pulse width, firing angle, and blocking signal. The outputs of the firing unit are the firing pulses given to thyristors in the bridge configuration. The firing pulse width was fixed at 1 ms. Synchronizing reference signals represented phase voltage waveforms at the HV side of the converter transformer. The phase voltage waveforms were passed through PLLs to synchronize the firing pulses to the fundamental frequency voltage. The line voltage signals were then synthesized inside the firing unit from the PLLs outputs. The firing angle input to

the bridge was given from the DC voltage controller. The block diagram of the bridge firing unit is shown in Fig. 5.3.

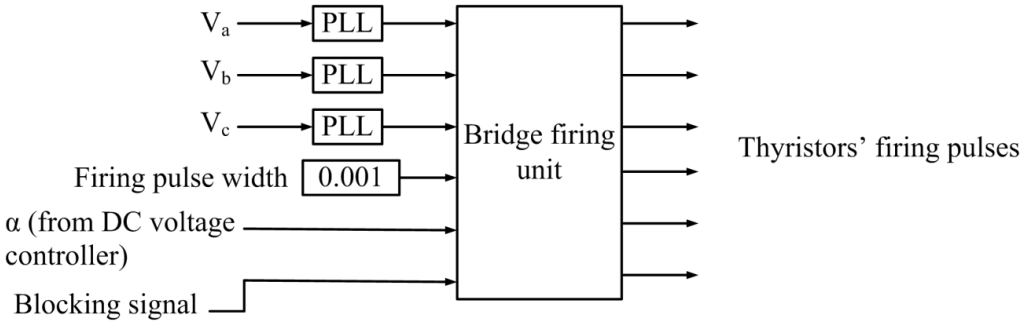


**Figure 5.3 6-pulse bridge firing unit**

### 5.2.2 Inverter Control System

The block diagram of inverter control system is shown in Fig. 5.4. As AC voltage control was adopted, the controlled parameter was the AC voltage, while the controlling parameter was the Modulation Index (MI). The minimum limit value of MI was set to 0.5, while the maximum limit was set to 1 so as to guarantee the operation in linear modulation region.

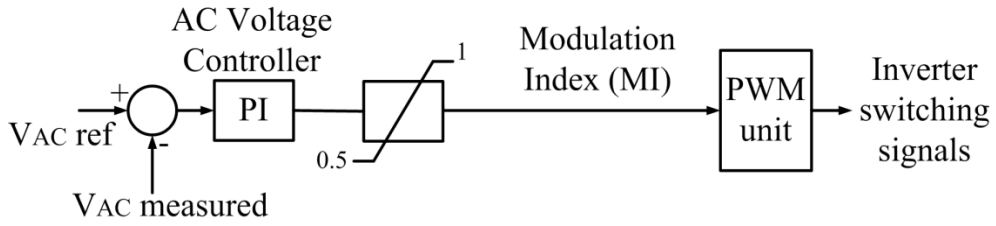


**Figure 5.4 Inverter control system**

## 5.3 Special Control Schemes

Special control schemes were developed to cope with transient and abnormal operating conditions such as light load starting and AC faults in RE network.

### 5.3.1 Light Load Starting Scheme

Light load starting proved to be problematic to the rectifier control system. Upon system starting at loads of less than 0.4 pu, a DC voltage collapse occurs and the system fails to start. The DC voltage collapse upon system starting at loads less than 0.4 pu is shown in Fig. 5.5. The DC voltage collapse is due to the DC voltage controller gains being inappropriate for system operation at light load.

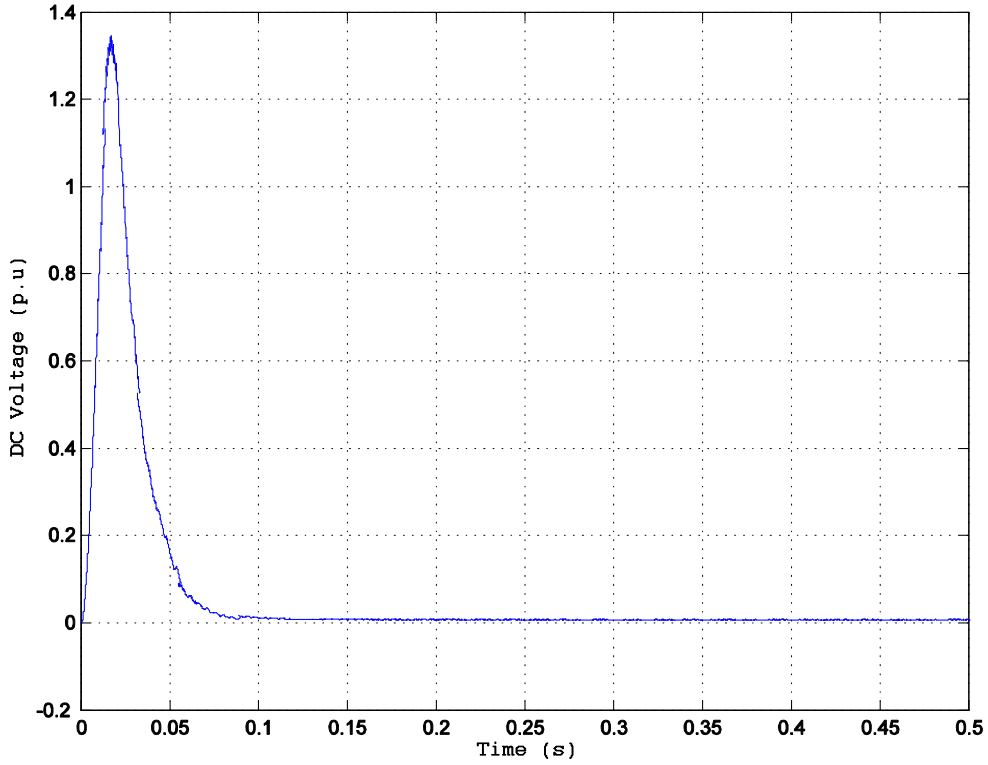


**Figure 5.5 DC voltage collapse upon light load starting**

In order to cope with light load starting condition, a starting scheme was developed. The scheme is shown in Fig. 5.6. The scheme makes use of another operating mode of the hybrid

system, in which the rectifier is operated at a fixed value of firing angle (i.e. open loop control for the rectifier control system). The principle of operation of the scheme is based on the detection of the DC voltage controller saturation which occurs in case of voltage collapse.

The sequence of operation for the starting scheme is explained as follows:

- Upon system starting at light load, a DC voltage collapse occurs, resulting in the saturation of DC voltage controller as well as the AC voltage controller at the inverter terminal.
- As a result of DC voltage collapse, the output voltage of the inverter is zero. This condition is detected by means of output voltage measurement at the inverter terminal. Then, the value of setpoint given to the AC voltage controller is reduced in order to reduce the level of saturation of the controller. In other words, the rate of rise of the modulation index above its upper limit is reduced by reducing the setpoint given to the controller.
- The saturation of the DC voltage controller is detected by a control circuit at the rectifier terminal. This control circuit deactivates the DC voltage controller and the rectifier is operated in fixed firing angle control mode. Upon switching to open loop control, a DC voltage starts to build up after the initial voltage collapse. As the DC voltage starts to build up, an output AC voltage starts to appear at the inverter terminal and the zero voltage condition is no longer present. The AC voltage setpoint is then ramped from its reduced value up to unity in the same fashion as in starting. In other words, a new starting is made but with the rectifier being operated in fixed firing angle mode.

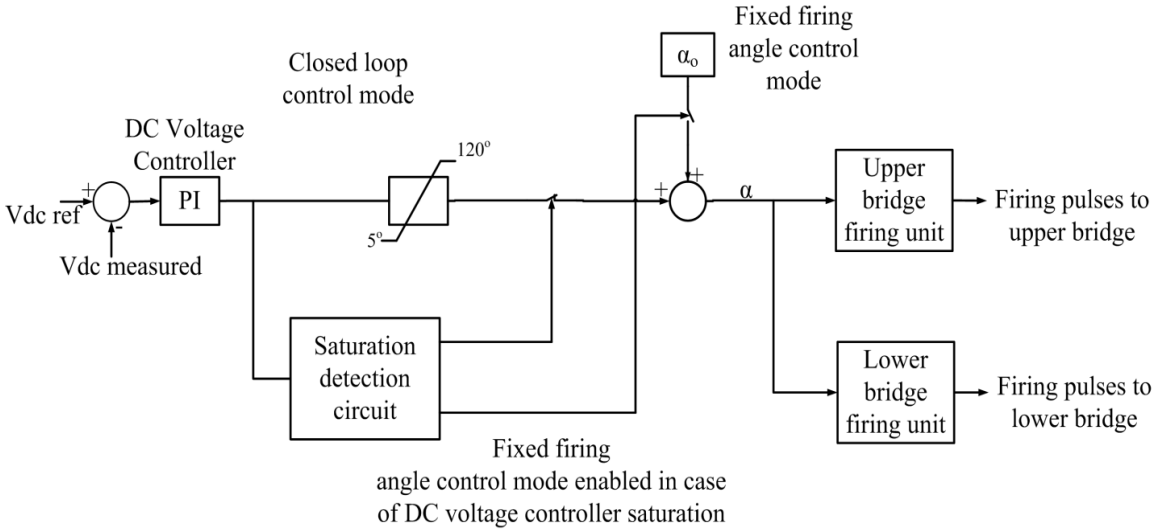


**Light load starting scheme at rectifier terminal**

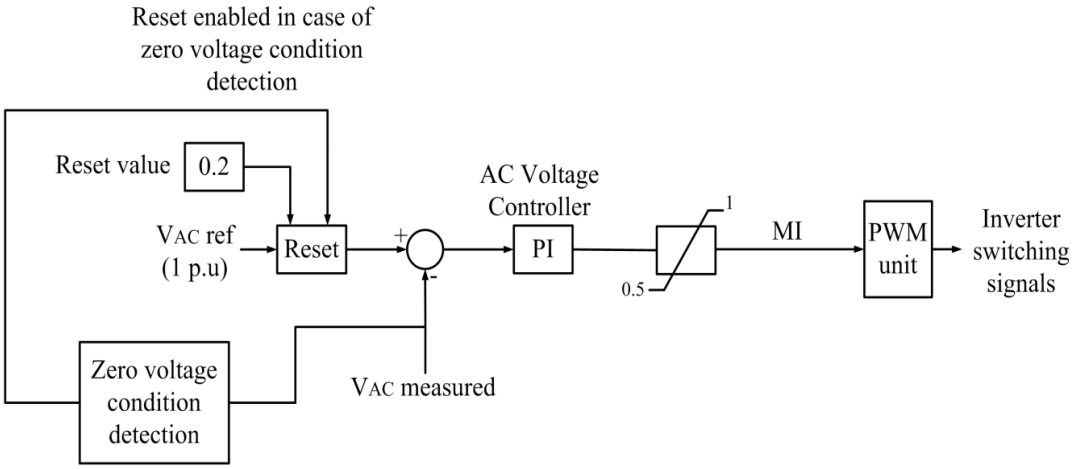


**Light load starting scheme at inverter terminal**

**Figure 5.6 Light load starting scheme**

## 5.3.2 Fault Handling Schemes

System faults at the RE network are considered among the most onerous transient disturbances that could be experienced by the transmission system. The duty of fault clearing is undertaken by CBs at the RE network, therefore the main issues of concern in system performance are the magnitudes of overvoltages at AC and DC sides during post-fault period, and the recovery time taken by the system to restore the nominal voltage and power at the RE load bus.

The AC fault handling scheme 1 is shown in Fig. 5.7. The scheme was designed with the objective of reducing the period of sustained overvoltage that takes place at the load bus upon fault clearing. This was obtained by maintaining the pre-fault value of voltage feedback during the fault to stabilize the controller output and prevent the saturation of its output. The scheme operation does not require any form of communication between rectifier and inverter terminals as both the measured signal and the control action are local to the inverter terminal and the RE network.

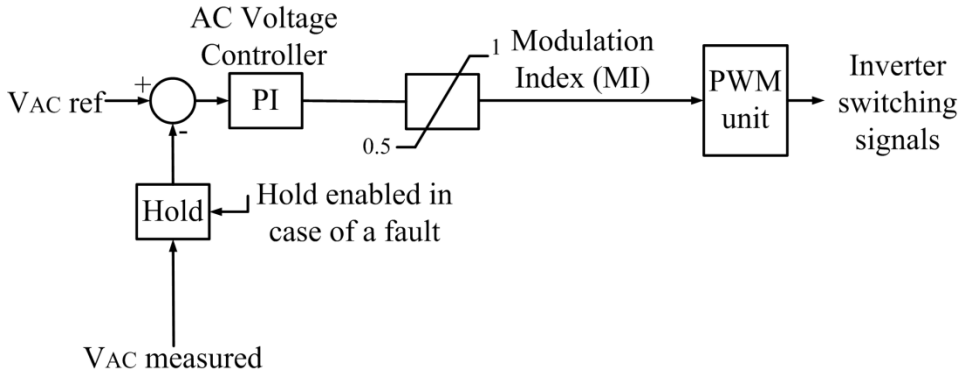


**Fig. 5.7 AC fault handling scheme 1**

The AC fault handling scheme 2 is shown in Fig. 5.8. The principle of operation for this scheme is based on the reduction of controllers' setpoints during fault period in order to reduce the post-fault overvoltage magnitude at DC and AC sides of the inverter, and to reduce the recovery time taken by the system to restore the normal voltage at the load bus. The reduction of AC voltage controller setpoint results in a lower rate of rise of MI during the fault period. Thus, the MI saturates for a brief period only upon fault clearing, resulting in a faster restoration of normal voltage at the bus. The reduction of DC voltage controller setpoint results in reduced magnitudes of overvoltages at DC and AC sides of the inverter. Since the scheme applies changes at both rectifier and inverter controllers, it is necessary to have a communication channel between both terminals in order for the scheme to be used.

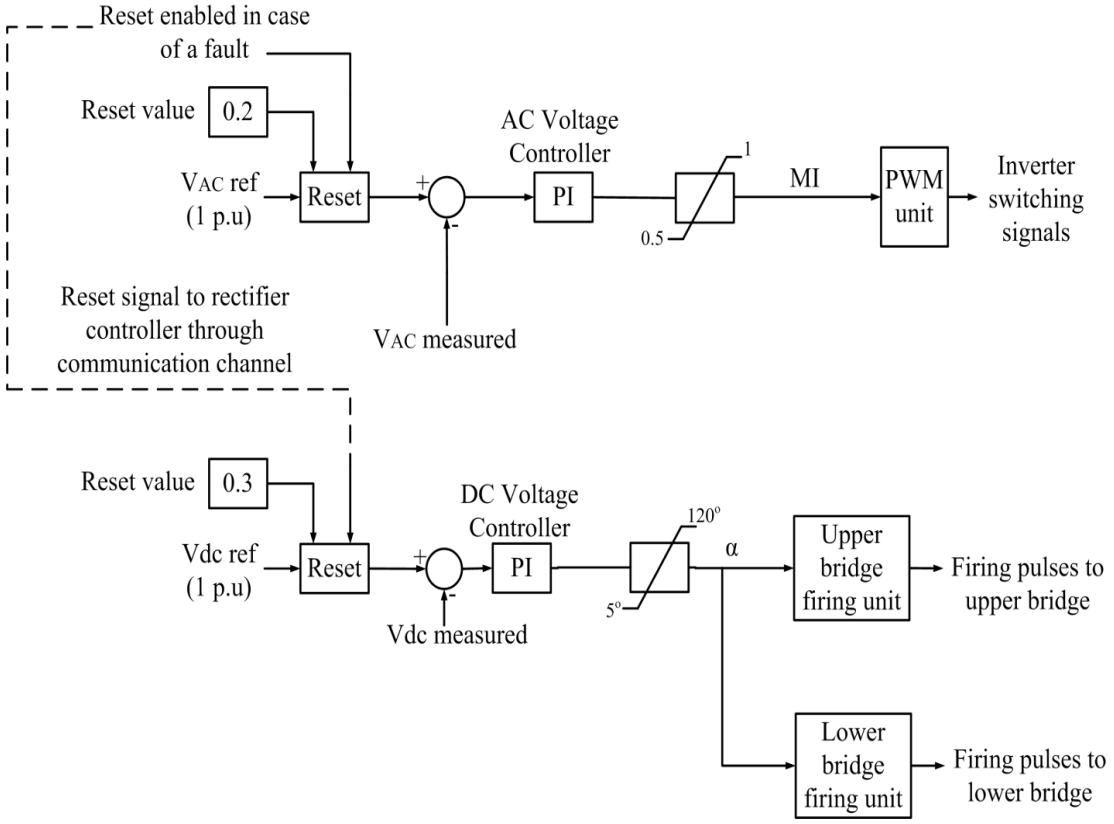


**Fig. 5.8 AC fault handling scheme 2**

### 5.3.3 Overcurrent Protection Scheme

Overcurrent protection aims at preventing the inverter valves damage by excessive current that results from overload or short circuits. Since valve current depends on the inverter total power output (MVA), it was necessary to keep the output MVA of the inverter below its rated value. In case of a passive network, however, the demand varies over time according to the connected load; therefore it is not practical to employ a secondary current controller since the current order is unknown and depends upon the load. Consequently, the overcurrent protection was made by voltage reduction in case of overloads, which in turn results in a reduction in the load current and the total MVA output of the inverter.

The block diagram of overcurrent protection scheme is shown in Fig. 5.9. The average valve RMS current is compared to the threshold value, which is typically the rated current of the valve. Upon detection of an overcurrent condition, a signal is generated for AC voltage setpoint reduction after a time delay of $T_{delay}$, which depends on the current rating of the valves and the efficiency of the cooling system.

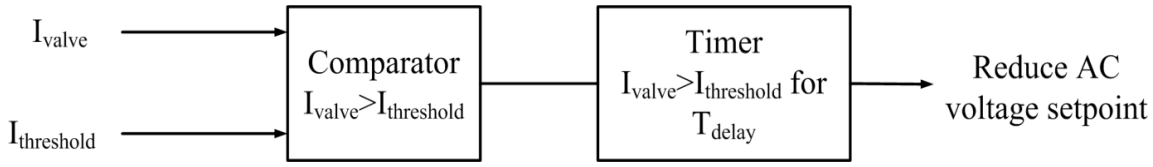


**Figure 5.9 Overcurrent protection scheme**

### 5.3.4 Oscillatory Mode Damping Scheme

The principle of operation for the oscillatory mode damping scheme depends on the inspection of magnitudes and frequencies of oscillations that are present in the control signal

of interest. In this case, it was chosen to apply the scheme to the firing angle signal, which is the output of the DC voltage controller.

The control signal typically has small oscillations around the steady state value in normal operation. During disturbances, however, the magnitude of oscillations increases as the system is transferred from one operating condition to another. The oscillations finally damp out as the system reaches its new steady state condition. Since both the magnitude and frequency of oscillations change during the disturbance, this change could be used to detect oscillatory modes of the system, in which a sustained oscillation occurs and persists without being attenuated by the system damping. The sustained oscillation condition typically occurs as a result of the system damping being too low; this could be handled by the alteration of controller gains to suit the new operating conditions.

The scheme operation was based on the detection of oscillations with frequencies less than or equal to 33 Hz in the firing angle signal. The threshold value of 33 Hz represents the upper limit of the range of frequencies that are characteristic to the sustained oscillations mode of the system. These frequencies vary between 24-33 Hz and they appear in the outputs of controllers when a large disturbance is experienced by the system, when the controller gains are not suitable for the post-disturbance operating conditions. The scheme operation is described as follows:

- The average value of the firing angle signal was calculated by an average calculator at a frequency of 20 Hz. This average value, being calculated at a relatively low frequency, is compared to the actual firing angle signal in order to detect the presence of large oscillations in the firing angle.

- Upon the occurrence of a disturbance causing the presence of sustained oscillations, the absolute value of the difference between the average and instantaneous values of the firing angle is increased and exceeds the narrow band of the firing angle fluctuation in steady state, selected at $\pm 2^{o}$.
- This will trigger the operation of a time period calculator, which calculates the period of each half-cycle of the oscillations in the firing angle.
- The periods of oscillations are compared to the threshold value of 33 Hz. Upon the detection of frequencies less than or equal to this value, a timer starts to count the total time for the presence of these oscillations.
- Once the total cumulative time for the presence of oscillations exceeds a threshold value of 0.05 s, a control signal is generated to re-tune the DC voltage controller gains. In this case, the proportional and integral gains are changed to 0.001 and 0.2 respectively. These new values of gains were found to yield a good system performance with no oscillations in case of light load operation.

The block diagram of oscillatory mode damping scheme is shown in Fig. 5.10.

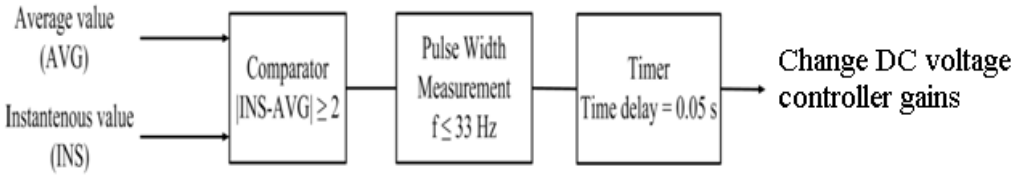


**Figure 5.10 Block diagram of oscillatory mode damping scheme**

## 5.4 Summary

In this chapter, the hybrid system specifications were presented. The control modes for the rectifier and inverter were selected; the control systems for rectifier and inverter were

presented and explained. In normal operating conditions, the selection of AC voltage control for the inverter terminal was necessary in order to provide a stable voltage source for the passive network at the receiving end, while the DC voltage was regulated by the DC voltage controller at the rectifier end. In order to handle abnormal and transient operating conditions, special control schemes were developed in order to maintain the stable operation of the hybrid system. This was achieved by providing a ride-through capability for the controllers, or by switching the system to another control mode which is suitable for the operating condition. The system performance under the selected control modes and the developed control schemes was tested and validated by EMTP-RV simulations presented in the chapter that follows.

# Chapter 6

# Results

## 6.1 System Starting

### 6.1.1 Starting at Full Load

The control objectives at system starting mainly included smooth starting by reducing the magnitude of overvoltage that occurs on both the DC side and the AC side, and fast starting by reducing the time taken by the system to attain steady state condition. The magnitude of overvoltage on DC side was limited to 1.15 pu as shown in Fig. 6.1 (a), while the magnitude of overvoltage on AC side (at the load bus) was limited to 1.16 pu as shown in Fig. 6.1 (e). The DC current experiences oscillations in the first 5 cycles and reaches its steady state value, after the charging of cable capacitance is ended, within 0.15 s as shown in Fig. 6.1 (b). The load power reaches its steady state value within 0.15 s as shown in Fig. 6.1 (d). The firing delay experiences large oscillations in the first 5 cycles and reaches its steady state value within 0.2-0.3 s as shown in Fig. 6.1 (c). It is also noticed that the starting scheme discussed in chapter 5 was not used in this case of starting at full load. The modulation index value is fixed at its lower limit of 0.5 for the first 3 cycles and reaches its steady state value within 0.2 s as shown in Fig. 6.1 (f).

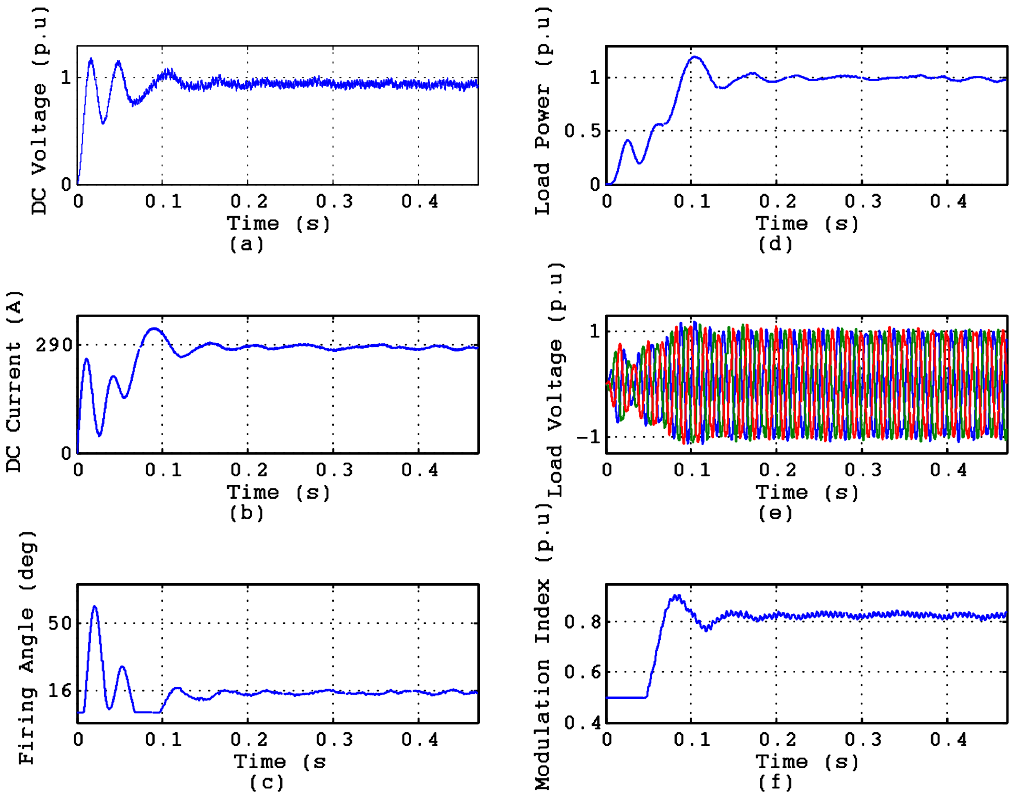


**Figure 6.1 System starting at full load**

The setpoints of DC voltage and AC voltage controllers are shown in Fig. 6.2. In order to achieve a smooth starting, the setpoint signal is given as a ramp reaching unity rather than a step at unity. The setpoint ramp times for DC voltage and AC voltage are 2 and 4 cycles respectively. An increased ramp slope would accelerate the voltage buildup but the magnitude of overvoltages will also increase. Although a faster starting could have been achieved by increasing the ramp slope of reference signals to the controllers, it was decided to limit the magnitude of overvoltages below 1.2 pu at the expense of a slight delay in

settling time. This was verified by simulation results, but due to brevity, the results are not included.

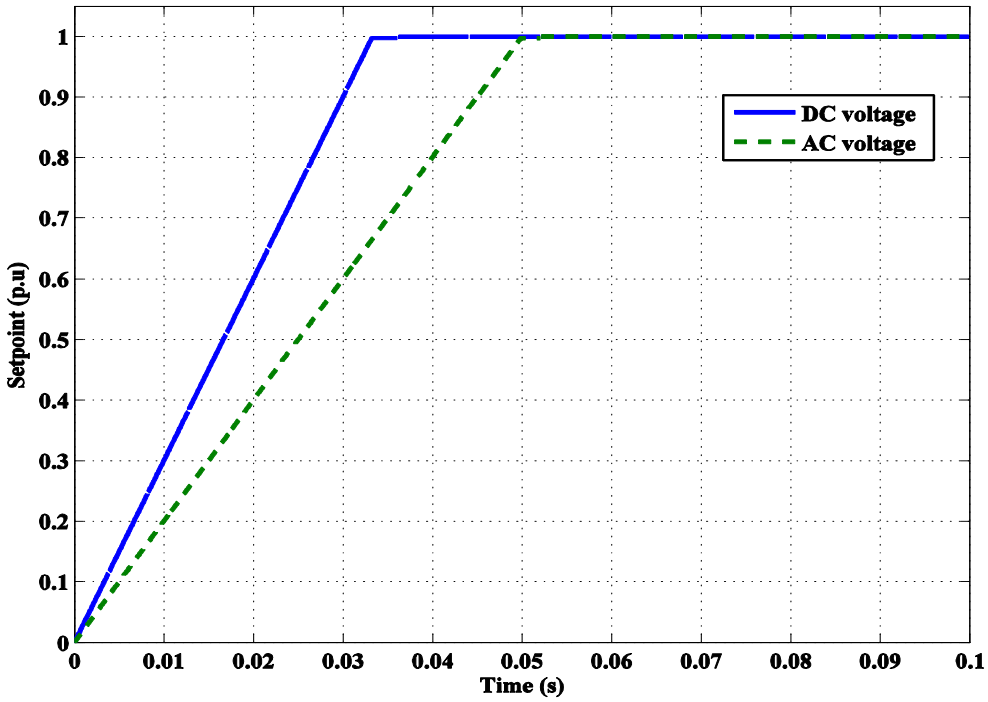


**Figure 6.2 DC voltage and AC voltage controllers' setpoints**

## 6.1.2 Starting at Light Load

Light load starting condition was handled using the starting scheme developed in section 5.3.1. The scheme achieves a re-starting of the rectifier after a DC voltage collapse caused by poorly tuned DC voltage controller gains. Since the controller is of fixed gain type, it is not possible to change the gains, and therefore it is necessary to operate the rectifier in fixed firing angle mode (open loop control mode) in order to restart the system. A sensitivity case involving a system starting at a load of 0.3 pu was conducted to test the performance of light

load starting scheme. The initial DC voltage collapse, shown in Fig. 6.3 (a), occurs within 5 cycles upon system starting. The operation of light load starting scheme then comes into effect after an intentional time delay of 0.1 s from the instant of voltage collapse. As the rectifier operation is switched into fixed firing angle control mode, at a firing angle of $40^{o}$, the DC voltage starts to build up after its collapse and settles at its new value of 0.8 pu within 5-6 cycles. The DC current is also settled within 5 cycles as shown in Fig. 6.3 (b). The load voltage settles within 6 cycles as shown in Fig. 6.3 (d). However, the load voltage experiences a sustained overvoltage that reaches 1.1 pu as a result of AC voltage controller saturation. This overvoltage remains present for 0.6 s after the restarting instant and causes an increase in the power received by the load which reaches 0.35 pu, as shown in Fig. 6.3 (c). It is worth mentioning that the system operation at full load is also possible with the rectifier being operated at fixed firing angle mode.

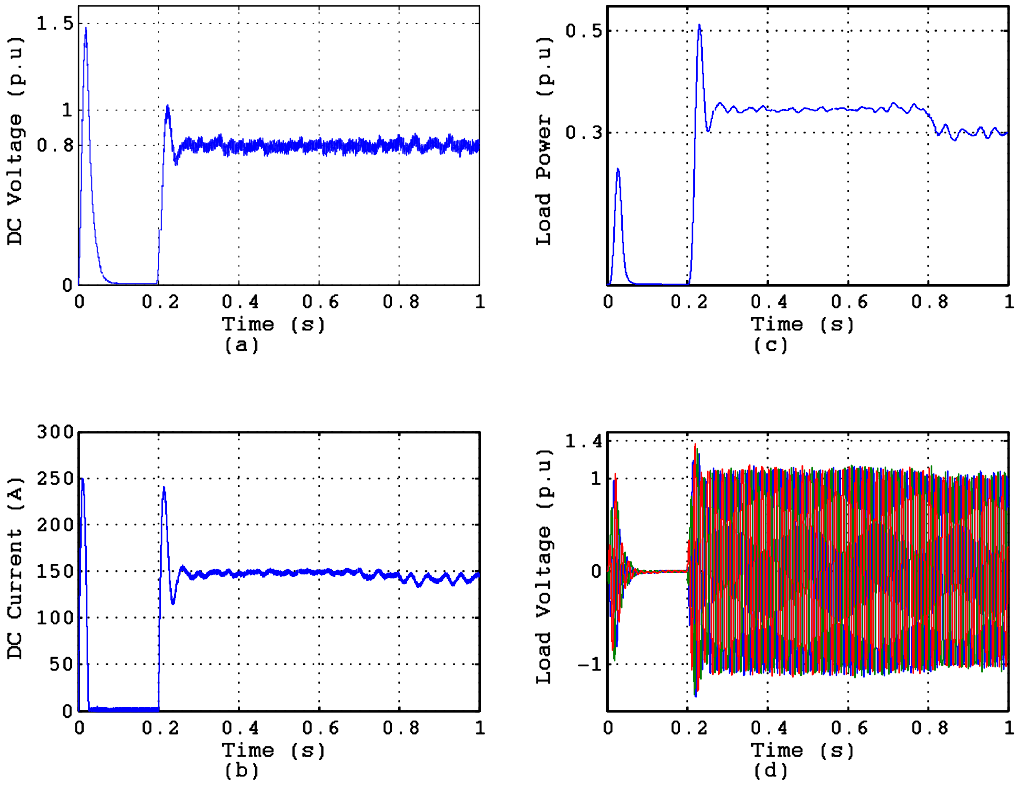


**Fig. 6.3 System starting at a load of 0.3 pu**

The control action of light load starting scheme is shown in Fig. 6.4. As the DC voltage controller saturates, a control circuit switches rectifier control to fixed firing angle mode after 0.1 s of controller saturation, as shown in Fig. 6.4 (a). The control action of the scheme at the inverter terminal is to reduce the AC voltage setpoint to 0.2 pu, as shown in Fig. 6.4 (c). This reduction in AC voltage setpoint helps reducing the level of saturation of AC voltage controller as shown in Fig. 6.4 (d) by decreasing the ramp slope of controller output. The controller output then starts to decrease as a result of DC voltage buildup and returns to its normal range of modulation index at 0.8 s of simulation time as shown in Fig. 6.4 (b). It is

worth mentioning that the rectifier is operated at such a high value of firing angle ($40^{o}$) since the DC voltage build-up could not take place at lower values of fixed firing angle. This is due to the AC voltage controller gains being poorly tuned for the light load condition.

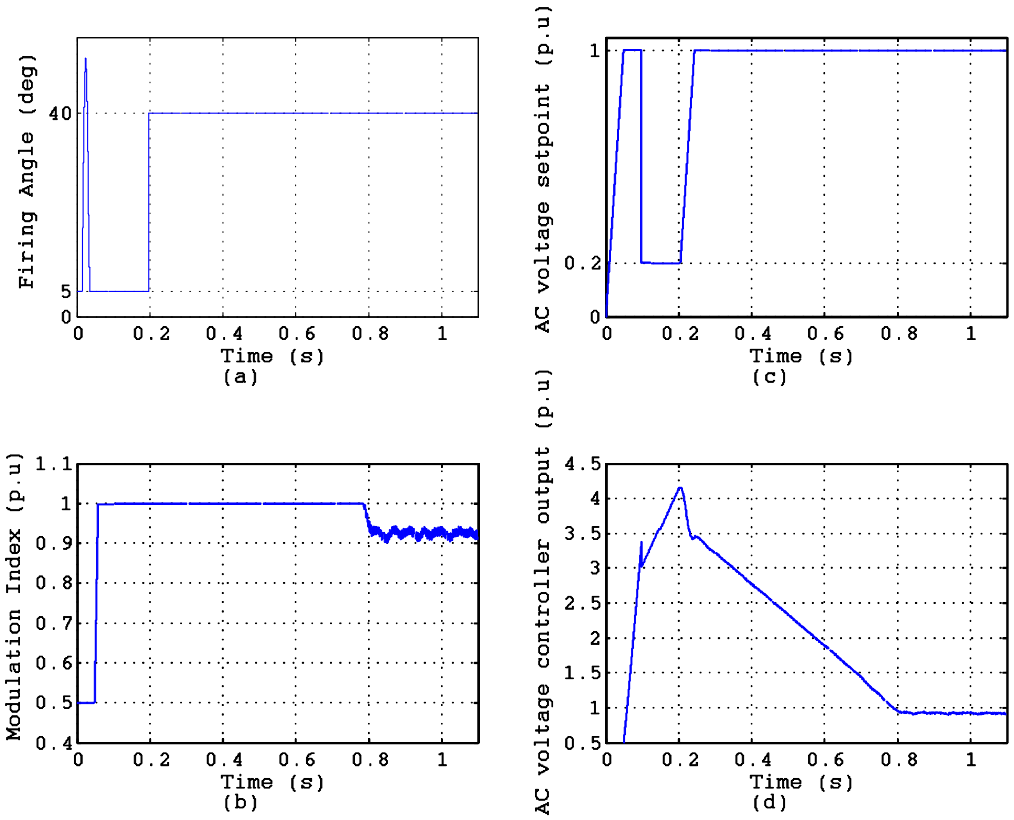


**Fig. 6.4 Firing angle, modulation index, AC voltage setpoint, and AC voltage controller output**

## 6.2 Load Disturbance

### 6.2.1 Negative Step Change

The effect of load disturbance on the system performance was one of the key issues investigated in the simulation study of the hybrid system. A sensitivity case involving a negative 0.2 pu step change is applied at 1 s of simulation time. The DC voltage experiences

some oscillations and settles within 4 cycles as shown in Fig. 6.5 (a). The load voltage experiences oscillations that settle within 5 cycles as shown in Fig. 6.5 (e). The DC current settles at the final value of 250 A within 5 cycles as shown in Fig. 6.5 (b). The load power tracks the step change and settles at the final value of 0.8 pu within 10 cycles as shown in Fig. 6.5 (d). The firing angle reaches its final value of $18^{o}$ within 7 cycles as shown in Fig. 6.5 (c). The modulation index reaches its final value of 0.8 within 6 cycles as shown in Fig. 6.5 (f).

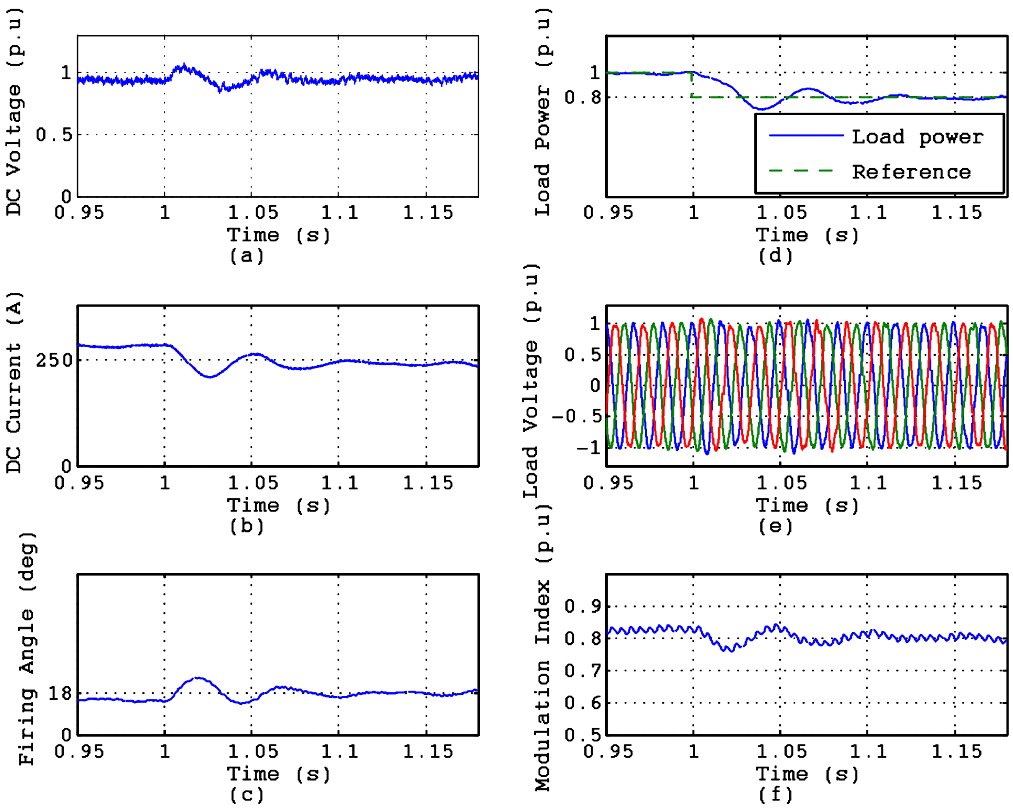


**Figure 6.5 0.2 pu negative step change in load power**

### 6.2.2 Positive Step Change

The simulation results for a sensitivity case of 0.2 pu positive step change in load are shown in Fig. 6.6. A step change is applied at 0.95 s of simulation time. The DC voltage experiences a momentary dip and settles within 5 cycles as shown in Fig. 6.6 (a). The load voltage also experiences a momentary dip and settles within 3 cycles as shown in Fig. 6.6 (e). The DC current reaches its final value of 280 A within 4 cycles as shown in Fig. 6.6 (b). The load power tracks the step change and settles at its final value of 1 pu within 8 cycles as shown in Fig. 6.6 (d). The value of firing angle oscillates and reaches its final value of $17^{o}$ within 9 cycles as shown in Fig. 6.6 (c). The modulation index reaches its final value of 0.81 within 10 cycles as shown in Fig. 6.6 (f). As far as the settling time of load power is concerned, the system response for a positive load disturbance (8 cycles) is less oscillatory than that for a negative step change (10 cycles).

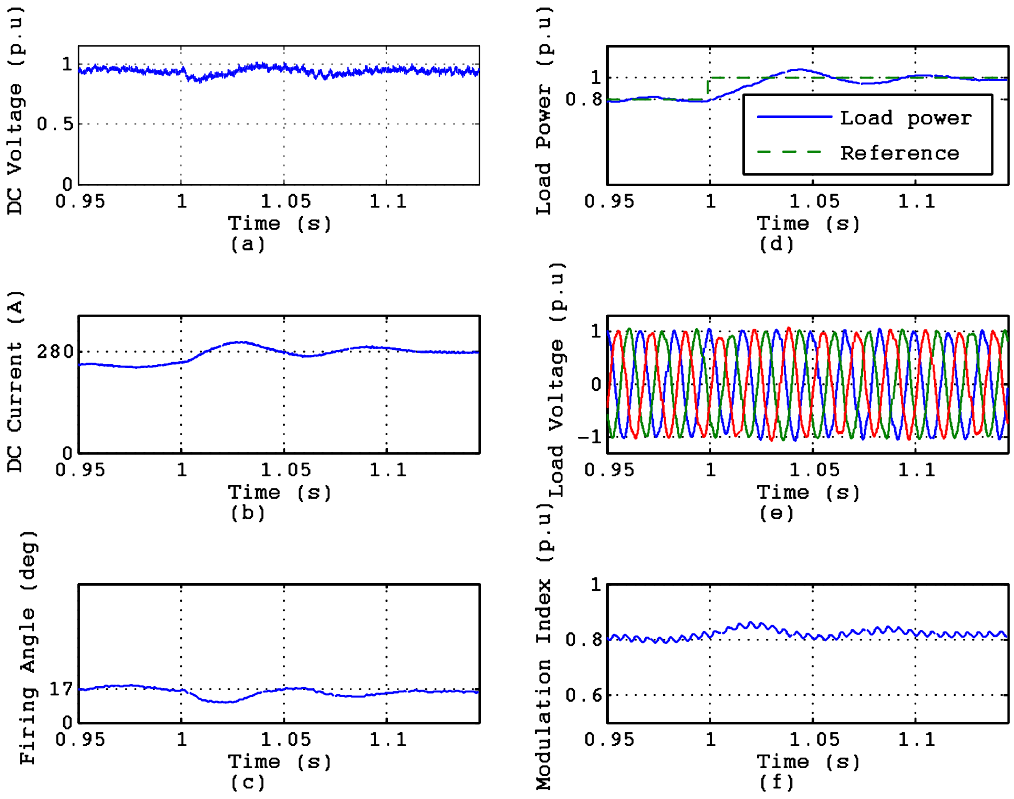


**Figure 6.6 0.2 pu positive step change in load power**

## 6.3 Three Phase Fault at Receiving-end Network

A three phase fault at the receiving-end network is the most severe transient disturbance that could occur in the system. The fault impedance was kept low at 10 Ohms in order to investigate the effects of such a severe fault on the performance of the controllers and the system in general. The fault handling schemes developed in section 5.3.2 were used to cope with the fault condition with the objective of reducing the magnitudes of overvoltages and the system recovery time. The simulation results for each of the developed schemes is

presented and analyzed and a performance comparison is made based on overvoltage magnitude and recovery time criteria.

### 6.3.1 Fault Handling by Scheme 1

Fig. 6.7 shows the simulation results for a three phase fault handled by scheme 1. The fault is applied at 1.2 s of simulation time and sustains for 0.1 s which is the approximate time taken by a high-speed circuit breaker to clear the fault. The recovery time of DC and AC voltages is measured from the instant of fault clearing at which the fault is removed from the system. The DC voltage experiences a severe dip that reduces its value to 0.2 pu as shown in Fig. 6.7 (a). Upon fault clearing, the magnitude of DC overvoltage reaches 2.4 pu. The recovery time for DC voltage is 10 cycles. The depressed load voltage reaches 0.1 pu as shown in Fig. 6.7 (e). Upon fault clearing, the magnitude of overvoltage at the load bus reaches 3.1 pu. The recovery time for load voltage is 11 cycles. The DC current increases and reaches a value of 900 A as a result of the power being dissipated in the fault, as shown in Fig. 6.7 (b). Upon fault clearing, the DC current is restored to its normal value within 4 cycles. The load power drops to zero during fault as shown in Fig. 6.7 (d). Upon fault clearing, the load power experiences a surge, due to the overvoltage at the load bus, and is quickly restored to its value within 10 cycles. The firing angle drops to its lowest limit of $5^{o}$ as a result of the abrupt decrease in DC voltage, and therefore the DC voltage controller output saturates. Upon fault clearing, the value of firing angle remains fixed at $5^{o}$ as a result of controller saturation. The firing angle is restored to its normal range within 0.44 s from the instant of fault clearing. The operation of fault handling scheme 1 is explained through the modulation index in Fig. 6.7 (f). The scheme prevents AC voltage controller output saturation by maintaining the pre-fault value of voltage feedback during the fault. Although a

slight increase in modulation index is made during the fault, due to the difference between the AC voltage setpoint and the instantaneous value of the AC voltage immediately prior to the fault, however the controller output saturation is prevented. Upon fault clearing, the modulation index experiences an abrupt drop reaching its low limit due to the DC overvoltage that takes place immediately after the fault clearing. It is also noticed that the post-fault value of modulation index is less than its pre-fault value. This is explained in light of the post-fault values of firing angle and DC voltage, since the DC voltage experiences a post-fault rise due to saturation of DC voltage controller and the low value of the firing angle. Thus, the post-fault value of the modulation index is expected to be higher for the same magnitude of output AC voltage.

In addition to the large values of post-fault overvoltages, the scheme causes the DC voltage saturation for a period of 0.37 s after fault clearing. This extended saturation of controller output would trigger the operation of the light load starting scheme that was used in section 6.1.2. In order to avoid this interference of control schemes, it is necessary to adjust the operation of the light load starting scheme in such a way that the scheme does not operate in fault situations. This would add, however, more complexity to the scheme operation.

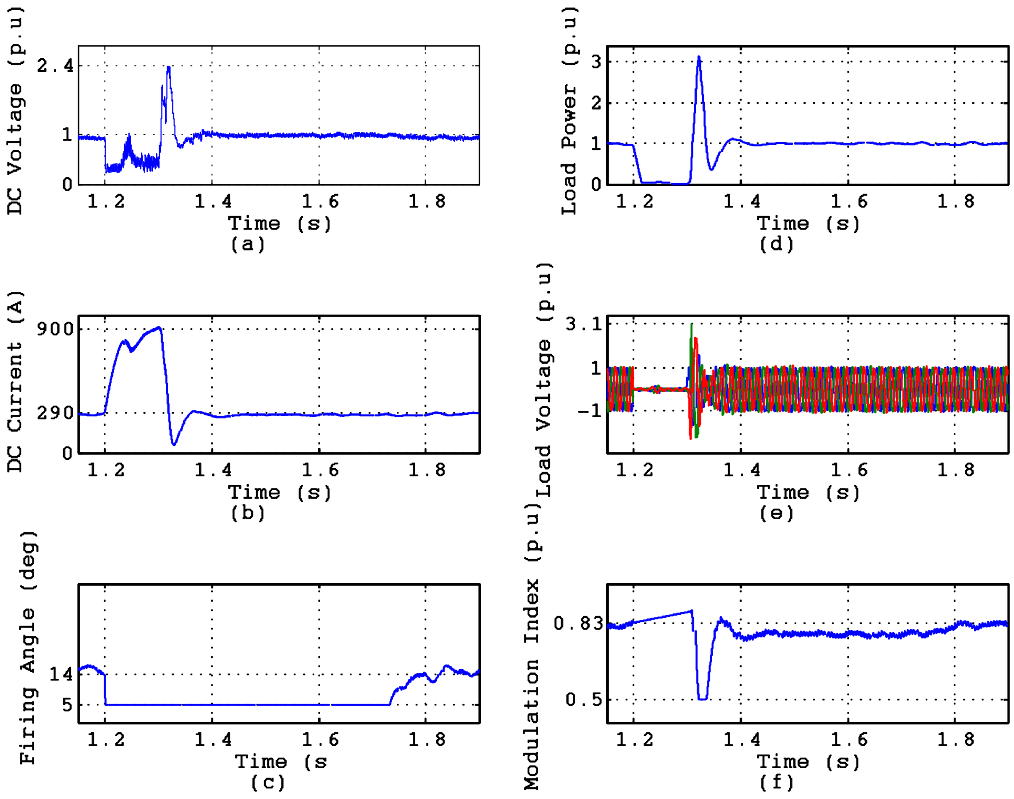


**Figure 6.7 Three-phase fault handled by scheme 1**

## 6.3.2 Fault Handled by Scheme 2

Fig. 6.8 shows the simulation results in case of a 3-phase fault handled by scheme 2. The fault is applied at 0.6 s of simulation time. The DC voltage is reduced to a value of 0.2 pu by means of the fault handling scheme as shown in Fig. 6.8 (a). Upon fault clearing, the DC voltage experiences a momentary rise to its rated value followed directly by an abrupt drop to its value during the fault. These rapid changes in DC voltage are due to the DC cable capacitance being recharged upon fault clearing and the restoration of the DC voltage setpoint to its normal value. The DC voltage recovers within 10 cycles. The depressed load

voltage during the fault reaches 0.1 pu as shown in Fig. 6.8 (e). Upon fault clearing, the magnitude of overvoltage at the load bus reaches 1.63 pu. The recovery time for load voltage is 10 cycles. Upon fault occurrence, the DC current initially experiences a drop and reaches a value of 40 A, as shown in Fig. 6.8 (b), due to the cable capacitance being discharged. The drop in DC current is then followed by a rise that reaches 550 A due to the power being dissipated in the fault. Upon fault clearing, The DC current is restored to its normal value within 10 cycles. The load power drops to zero during the fault as shown in Fig. 6.8 (e). Upon fault clearing, the load power experiences a surge that reaches 1.4 pu due to the overvoltage at the load bus, and settles within 12 cycle. The firing angle experiences a surge upon fault occurrence, as shown in Fig. 6.8 (c), due to the reduction in DC voltage setpoint by the fault handling scheme. Upon fault clearing, the firing angle experiences some oscillations and settles at its final value of $16^{o}$ within 9 cycles. The effect of fault handling scheme 2 is explained through the modulation index in Fig. 6.8 (f). Upon fault occurrence, the reduced AC voltage setpoint results in an abrupt drop of the modulation index to its low limit. Since the voltage at the load bus is less than the reduced setpoint of 0.2 pu, the modulation index starts to rise during the fault until it reaches its high limit and the AC voltage controller saturates. The scheme, however, prevents a faster saturation of the AC voltage controller output and consequently a longer period of sustained overvoltage at the load bus after fault clearing. This is proven by the fast restoration of modulation index to its normal value within 9-10 cycles.

The use of fault handling scheme 2 reduces the magnitudes of post-fault overvoltages and prevents saturation of controllers. Moreover, the firing angle response shows no extended period of controller saturation at its low limit. Therefore it is not prohibitive to run fault

handling scheme 2 and the light load starting scheme together. In other words, the simultaneous operation of fault handling scheme 2 and light load starting scheme does not require a special adjustment of either of the schemes for the purpose of coordination. On the other hand, the use of fault handling scheme 1 requires the adjustment of light load starting scheme, as shown in section 6.3.1. Therefore, it is strongly recommended to use fault handling scheme 2 and not fault handling scheme 1 for AC network fault handling.

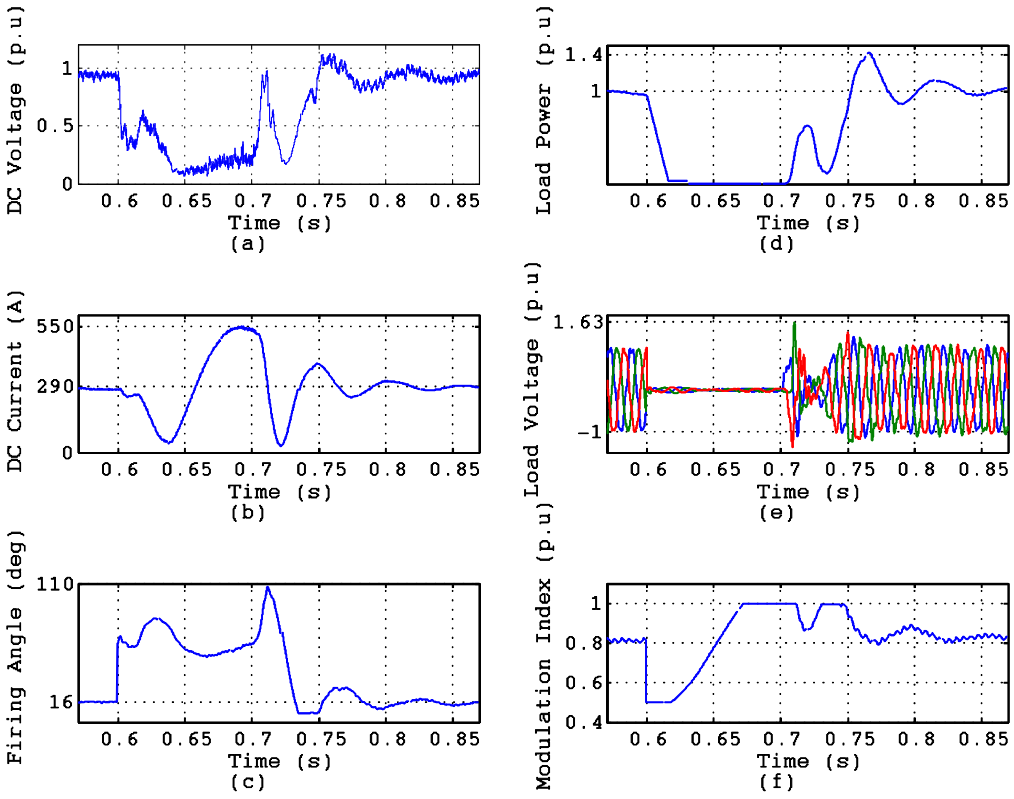


**Figure 6.8 Three-phase fault handled by scheme 2**

The setpoints of DC and AC voltage controllers are shown in Fig. 6.9. The principle of operation of fault handling scheme 2 is based on the reduction of controllers' setpoints during

the fault in order to avoid excessive controller output saturation and to reduce the magnitude of post-fault overvoltages. The ramp slope of AC voltage setpoint is made less than that of DC voltage setpoint in order to reduce the magnitude of post-fault overvoltage at the load bus and to allow the recovery of DC voltage before full AC voltage is applied at the load bus.

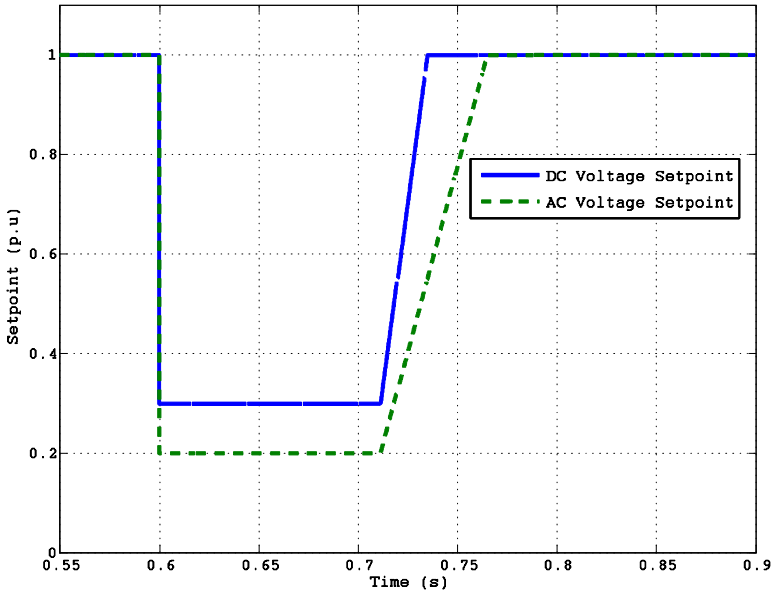


**Figure 6.9 DC and AC voltage controllers setpoints using scheme 2**

## 6.4 Inverter Overcurrent Protection

### 6.4.1 Overload Protection

The overcurrent protection scheme was tested by a sensitivity case of an overload of 30% in magnitude that lasts for 1 second. The RMS current measurement shown in Fig. 6.10 (a) was used to detect the overcurrent condition, which was defined as the average valves' current being higher than 200 A for 0.4 s. The overload flag was then set to high as shown in

Fig. 6.10 (d). The scheme acted by reducing the AC voltage setpoint to 0.88 pu as shown in Fig. 6.10 (c). Fig. 6.10 (b) shows the effect of the scheme operation, which results in limiting the inverter output to its rated value after a short overload during the time delay period. This time delay is used to prevent the scheme operation in case of transients and momentary overloads. The length of time delay depends upon the current rating of inverter valves, as well as the efficiency of the cooling system used for heat removal from the valves.

Upon the end of overload period, the inverter MVA output, shown in Fig. 6.10 (b), is used to reset the overload flag and control action of overload scheme by restoring the AC voltage setpoint to its normal value of 1 pu after a time delay of 0.12 s as shown in Fig. 6.10 (d) and 6.10 (c), respectively. The valve current is kept below the limit of 200 A as shown in Fig. 6.10 (a).

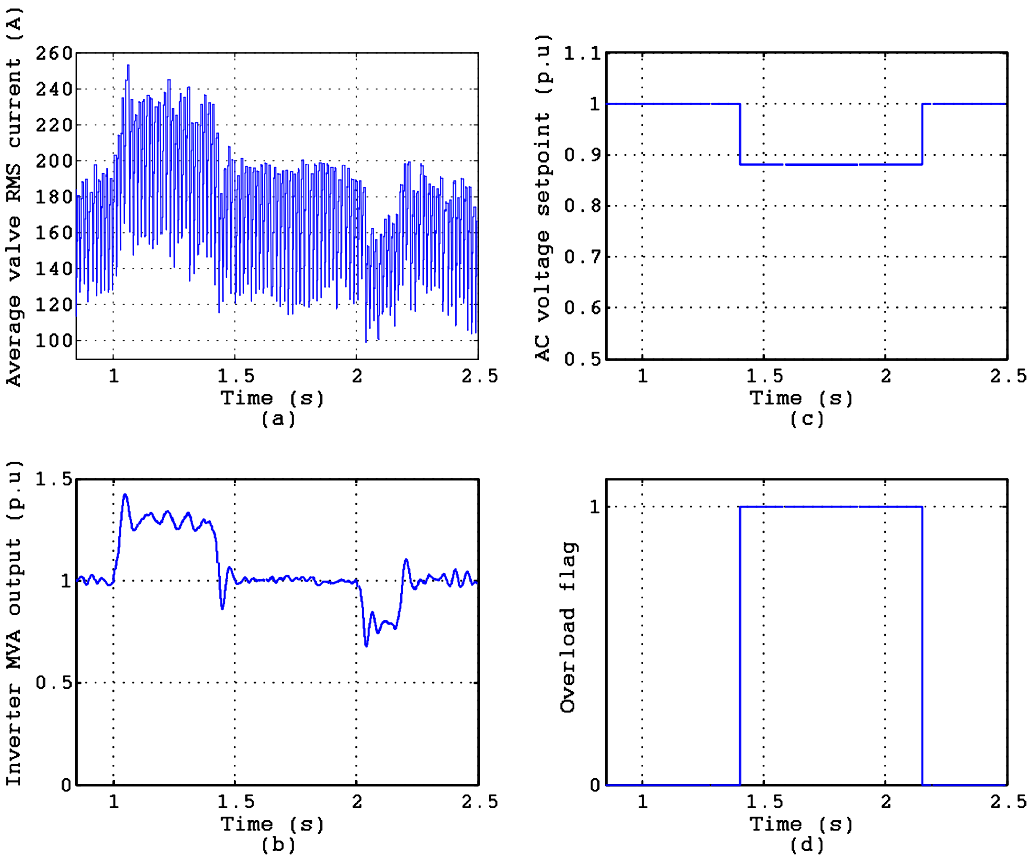


**Figure 6.10 Overcurrent protection scheme operation**

The impact of AC voltage setpoint reduction on DC voltage is an oscillation that settles within 4-5 cycles, as shown in Fig. 6.11 (a). The modulation index also experiences some oscillations that settle within 4 cycles as shown in Fig. 6.11 (b). The oscillations in load power settle within 6-7 cycles as shown in Fig. 6.11 (c). The load voltage tracks the change in setpoint within 7 cycles as shown in Fig. 6.11 (d).

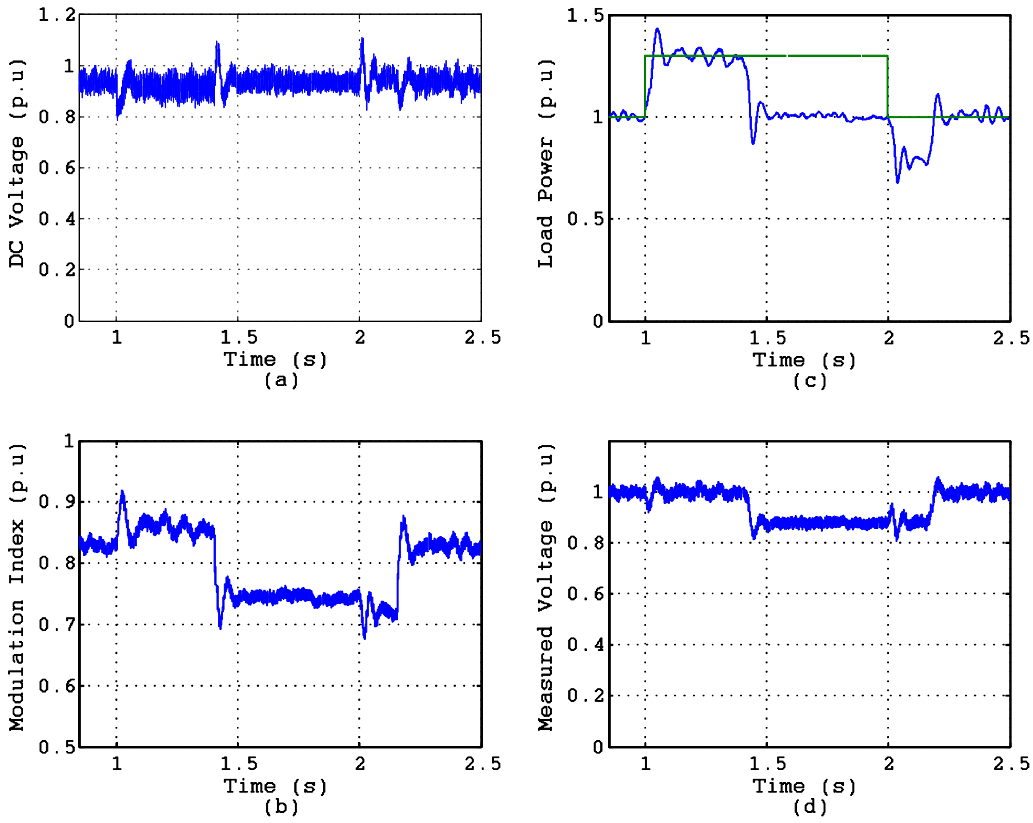


**Figure 6.11 Impact of overcurrent protection on system performance**

## 6.4.2 Short Circuit Performance of Fault Handling Schemes

The objectives of fault handling schemes are mainly to reduce the magnitude of post-fault overvoltages and the voltage recovery time. Moreover, the magnitude of short circuit current flowing through the valves is another criterion for assessing the performance of fault handling schemes. In case of short circuits, the currents in inverter valves are different from each other due to possible differences in fault impedance and short circuit current path. Thus, it was necessary to find the current in each individual valve in the inverter.

The RMS valve currents in case of 3-phase fault handled by fault handling scheme 1 are shown in Fig. 6.12. The transient (short-time) current carrying capability of the inverter valves shall not be less than the highest RMS current reached during the fault for a period greater than or equal to the fault clearing time (taking the design for the worst case scenario). Thus, the short-time rating of inverter valves using scheme 1 shall not be less than 950 A for 0.1 s. The ratio of the highest short circuit current to rated valve current is therefore 4.25.

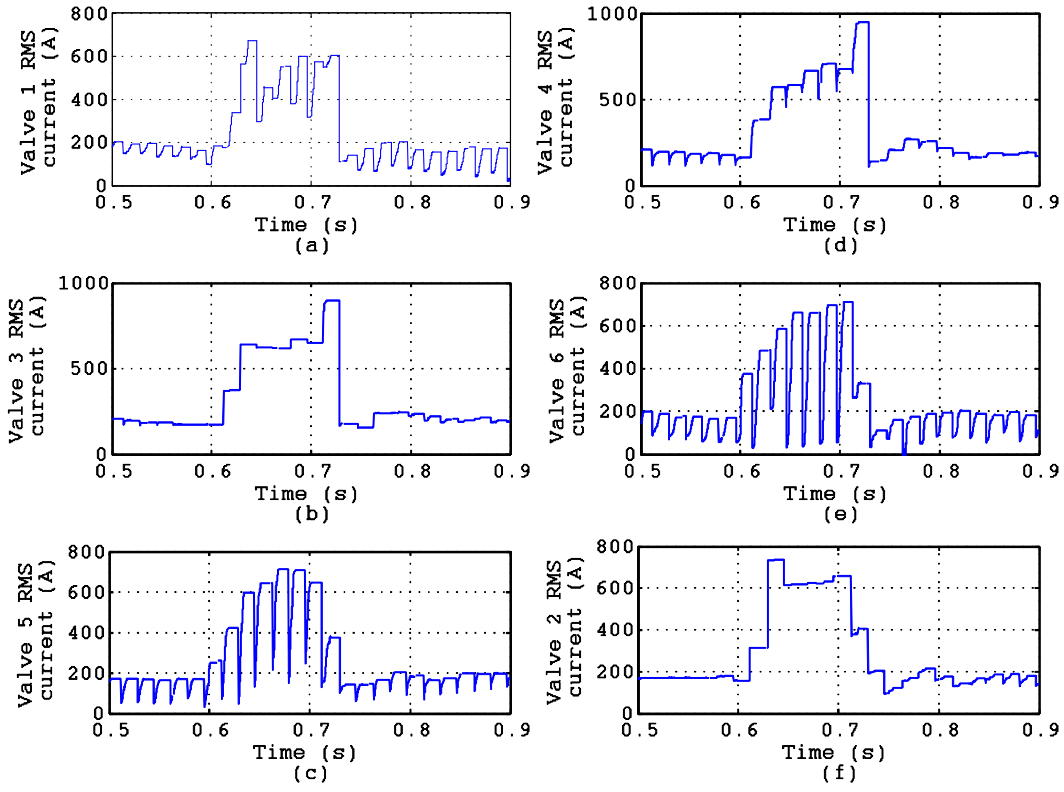


**Figure 6.12 Short circuit currents in inverter valves upon the use of fault scheme 1**

The RMS valve currents in case of a 3-phase fault handled by fault handling scheme 2 are shown in Fig. 6.13. Based on the short-time rating definition mentioned above, the short-time

rating of the inverter valves shall not be less than 600 A for 0.1 s. Thus, the ratio of highest short circuit current to rated valve current is 3. It shows that the short-time rating of the valves using fault handling scheme 2 is less than that when using scheme 1. Thus, the short circuit current criterion also favors the use of fault handling scheme 2.

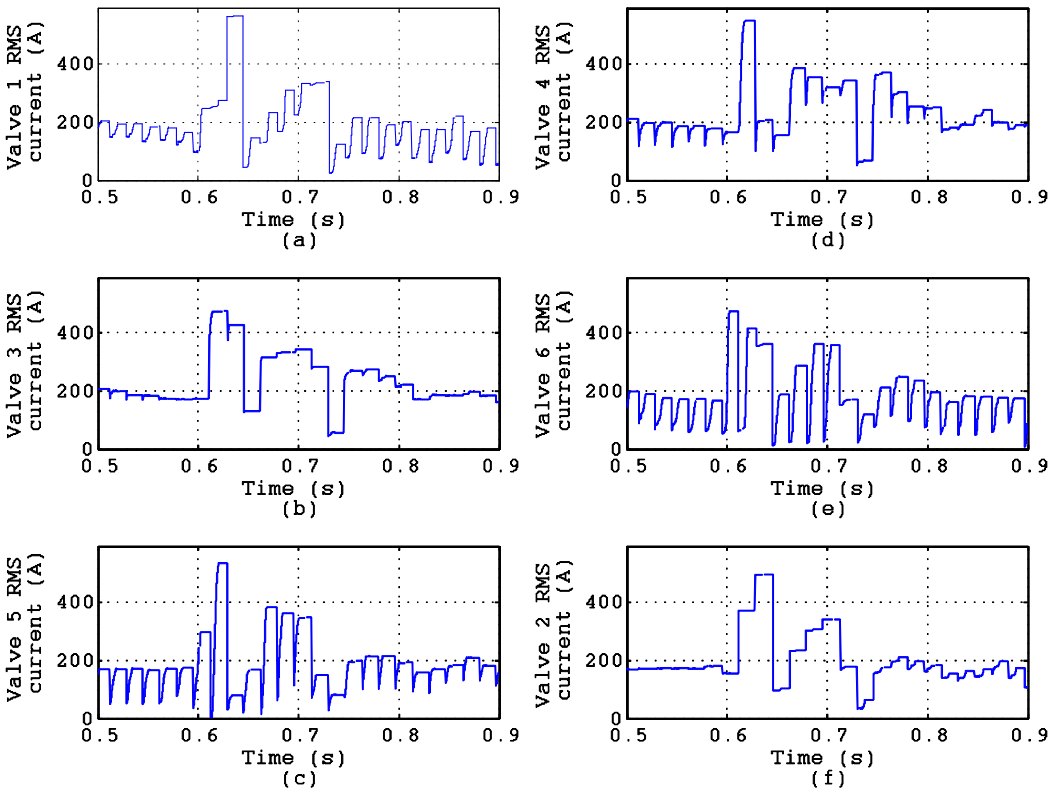


**Figure 6.13 Short circuit currents in inverter valves upon the use of fault handling scheme 2**

## 6.5 Oscillatory Mode Damping

The oscillatory mode damping scheme developed in section 5.3.4 was used to handle a load shedding situation in which 50% of the load is suddenly disconnected from the system

at 1 s of simulation time. This large load disturbance triggered an oscillatory mode in which sustained oscillations exist in the firing angle. Consequently, the oscillations were reflected on the DC voltage and modulation index and the system was trapped into a state of sustained oscillations that cannot be damped. The oscillatory mode damping scheme then intervenes to adjust the DC voltage controller gains and restore the system to its normal operation.

The first stage in the scheme operation is made by subtracting the average value of firing angle from its instantaneous value, shown in Fig. 6.14 (a). The absolute value of this subtraction, shown in Fig. 6.14 (b), represents the deviation of the instantaneous signal value from its average value. This deviation, when exceeding $2^{o}$, is used to generate the pulses shown in Fig. 6.14 (c). The width of each individual pulse is then measured as shown in Fig. 6.14 (d). The width of each individual pulse is indicative of the frequency of oscillation that takes place in the firing angle.

The load disturbance, applied at 1 s of simulation time, results in a series of un-damped oscillations that appear in the firing angle, as shown in Fig. 6.14 (a). Although the magnitude of oscillations appears to be diminishing at 1.45 s, however it quickly grows again and it could be noticed that the system has entered a state of un-damped oscillations. The frequency of these oscillations is compared to the threshold value of 33 Hz by the half-cycle width measurement in Fig. 6.14 (d). A half cycle width of 0.015 s or more will result in a cumulative off-delay timer to count (the half cycle width of 0.015 s corresponds to the half cycle width of 33 Hz oscillation). When the timer counts 0.05 s elapsed with these oscillations being present, a control signal is generated to change proportional and integral gains of DC voltage controller to 0.001 and 0.2 as shown in Fig. 6.14 (a) and (b) respectively.

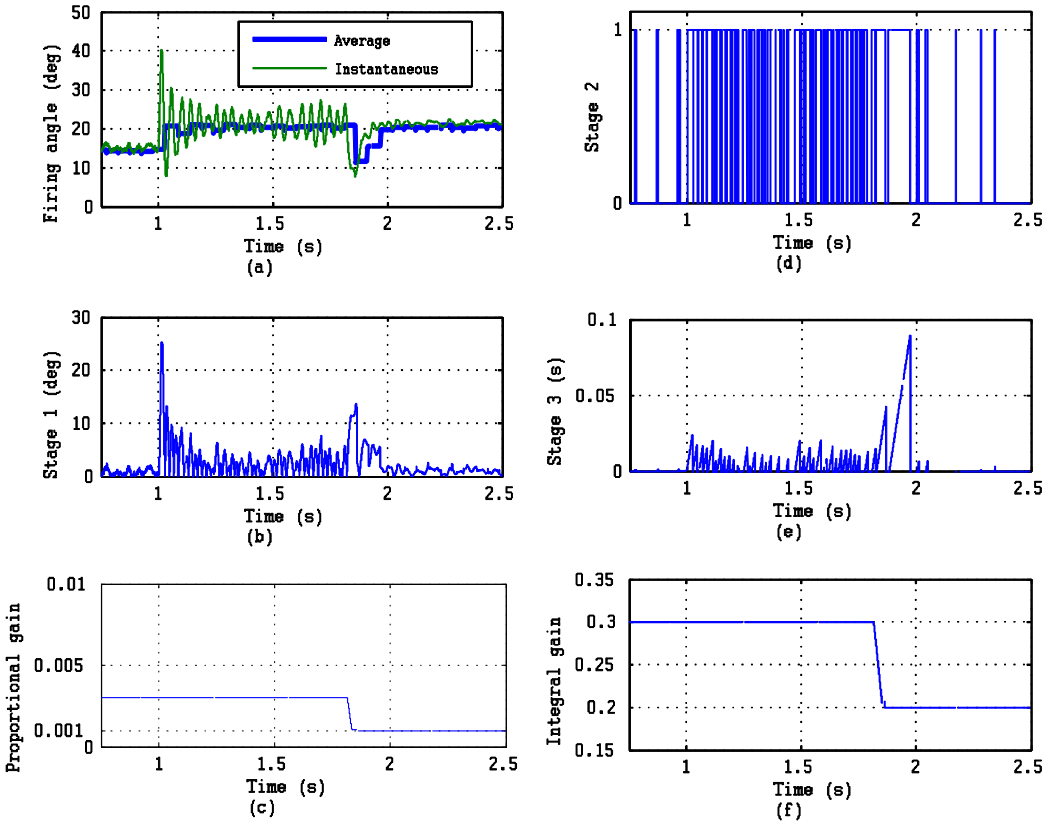


**Figure 6.14 Oscillatory mode damping scheme operation**

The effect of the oscillatory mode damping scheme on the system performance is shown in Fig. 6.15. As the DC voltage controller gains are changed at 1.8 s of simulation time, the firing angle experiences a drop and settles at its new steady state value of 22 within 0.2 s, as shown in Fig. 6.15 (a). After experiencing oscillations for about 1 s after the initial disturbance, the DC voltage settles at its new steady state value of 0.98 pu within 0.3 s as shown in Fig. 6.15 (b). The modulation index settles at a new lower value of 0.78, as shown in Fig. 6.15 (c), as a result of the increase of the DC voltage. The oscillations in load power are damped out within 0.3 s of the change in DC voltage controller gains as shown in Fig. 6.15 (d). The overall effect of the scheme operation on the system is the attenuation of the

oscillatory mode that arose as a result of the large load disturbance applied at 1 s. The scheme succeeded in damping out oscillations in DC voltage and restored its value within the allowable voltage regulation limit of ±5%.

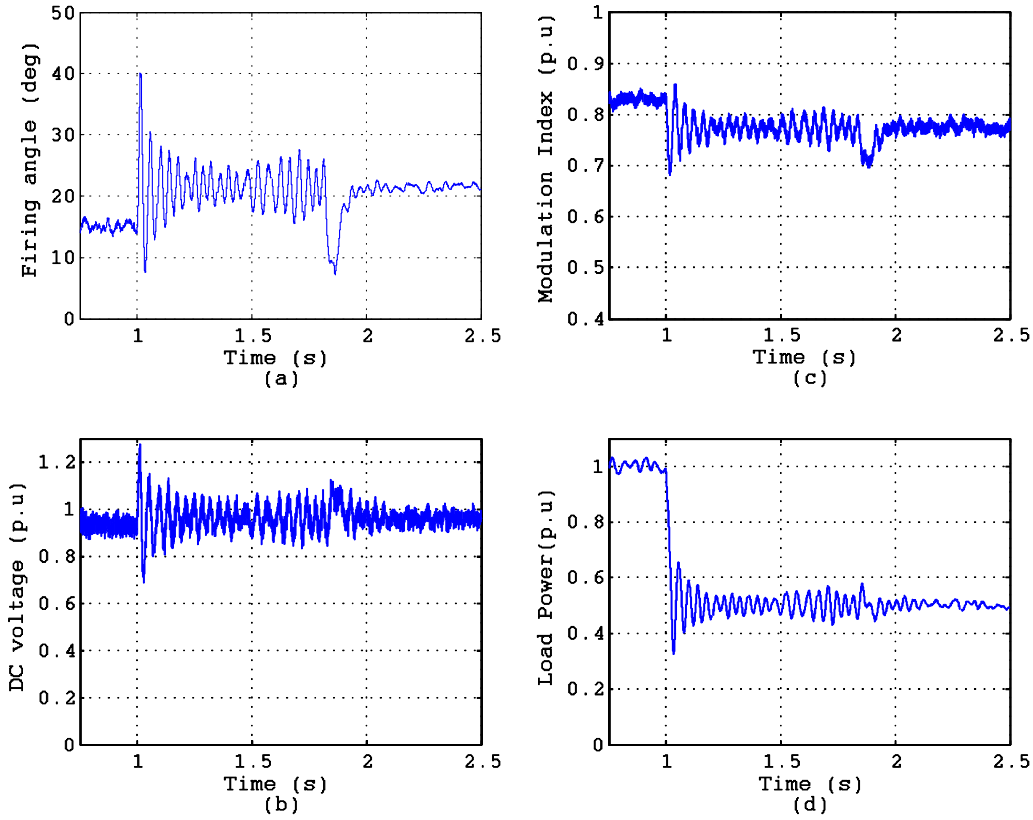


**Figure 6.15 Effect of oscillatory damping scheme on the system performance**

## 6.6 Summary

In this chapter, the system performance was investigated in both steady state and transient operating conditions. The system response to small signal disturbances, such as load changes, was presented and analyzed. The system performance in transient conditions under the

developed control schemes was presented and discussed. The main concluding point of the chapter is that the use of fault handling scheme 2 achieves a better response in terms of overvoltages magnitudes, system recovery time, and short circuit current in inverter valves.

# Chapter 7

# Conclusions and Future Work

## 7.1 Conclusions

The thesis presents a hybrid HVDC transmission system that has a LCC at its sending-end and a VSC at its receiving-end. The VSC supplies a passive network at the receiving-end. Therefore the receiving-end load relies solely on the VSC. Consequently, the VSC had to be operated in AC voltage control mode, while the LCC was operated in DC voltage control mode.

Fixed-gain PI controllers are used to regulate the controlling parameters at the rectifier and inverter terminals. The firing angle is regulated by the DC voltage controller at the rectifier terminal, while the modulation index is regulated by the AC voltage controller at the inverter terminal. Since the receiving-end network is passive, direct control of VSC is used and the controlling variable is the modulation index only. The use of direct control is justified in this particular case of power supply to a passive network since direct control is simple and cheap, and since there is neither a requirement of independent control of active and reactive power, nor a requirement of power reversal between both ends of the DC tie.

Although fixed gain controllers with properly-tuned gains provide a satisfactory system performance and appropriate response to load changes, their main disadvantage is their inability to handle the system upon significant changes in operating conditions. In other

words, the PI controller gains become inappropriate to provide a satisfactory system performance upon large changes in load or AC fault situations.

Since PI controllers are unable to handle abnormal conditions, such as starting at light load, and transient conditions, such as an AC fault at the receiving-end network; special control schemes are developed in order to handle these conditions. The objective of these control schemes is to maintain a stable system operation during abnormal conditions and to allow the system to ride through the disturbances and recover quickly. The schemes operate either by intervening with the normal control mode to achieve the desired control objective, or by switching the system to a different control mode. The second developed fault handling scheme is the option of choice as it reduces the magnitude of post-fault overvoltage to 1.63 pu with a voltage recovery time of 10 cycles, and as it does not interfere with light load starting scheme. This fault handling scheme, however, requires establishing a communication channel between rectifier and inverter terminals.

The hybrid HVDC system is applicable to a wide number of existing HVDC installations where the power flow over the DC link is predominantly unidirectional. An ideal application of the hybrid system is found where the receiving-end network is passive, since a VSC does not need an active voltage source to commutate against. This makes the hybrid system a perfect choice for power supply to islands and remote communities where there is no connection to the utility grid.

The major contributions of this thesis are the following:

1. The development of a simulation model for the hybrid HVDC system in EMTP-RV simulation environment.

2. The development of two fault controllers to handle 3-phase faults that may occur in the receiving-end network.
3. The development of a control scheme to enable system starting and operation at light load conditions.
4. The development of an oscillation damping scheme to handle large load disturbances.

## 7.2 Future Work

The following aspects remain to be investigated in the future work of this project:

1. Use of advanced control strategies (fuzzy logic or adaptive control) in rectifier and inverter controllers: this may be able to improve the system performance and its dynamic response to various disturbances. It may also eliminate the need for the communication link between rectifier and inverter terminals.
2. Extension of the system into a multi-terminal one: this is done by adding a second inverter terminal supplying an active network. An important aspect of this future research is to investigate the performance of vector control at the inverter terminal supplying the active network.
3. Diversification of load models used at the receiving-end terminal: an important load type to be used in this future research is the induction motor load. This is expected to improve the results and give a better insight on the performance of the hybrid system, as the load would

become a combination of fixed-impedance and dynamic loads, which is the situation found in real world power system loads.

# References


[1] Erik Koldby, and Mats Hyttinen, “ Challenges on the Road to an Offshore HVDC Grid ”, Nordic Wind Power Conference, Bornholm, Denmark, September 2009.

[2] Kenneth Johanesson, Anders Gustafsson, Johan Karlstrand, and Marc Jeroense, “ HVDC Light Cables for Long Distance Grid Connection ”, European Offshore Wind Conference, Stockholm, Sweden, September 2009.

[3] Gunnar Asplund, “ Electric Transmission System in Change ”, IEEE Power Electronics Specialists Conference, Rhodes, Greece, June 2008.

[4] Gunnar Asplund, Kjell Eriksson, and Ove Tollerz, “ HVDC Light, a Tool for Electric Power Transmission to Distant Loads ”, VI SEPOPE Conference, Salvador, Brazil, May 1998.

[5] Kala Meah, and Sadrul Ula, “ Comparative Evaluation of HVDC and HVAC Transmission Systems ”, IEEE Power Engineering Society General Meeting, Tampa, FL USA, June 2007.

[6] Shu Wang, Jinxiang Zhu, Lan Trinh, and Jiuping Pan, “ Economic Assessment of HVDC Project in Deregulated Energy Markets ”, Electric Utility Deregulation, Restructuring and Power Technologies Conference, Nanjing, China, April 2008.

[7] Zaki E. Al-Haiki, and Ahmed N. Shaikh Nasser, “ Power Transmission to Distant Offshore Facilities ”, Petroleum and Chemical Industry Conference, Anaheim, CA USA, September 2009.

[8] B. R. Andersen, “ HVDC Transmission-Opportunities and Challenges ”, 8th IEE International Conference on AC and DC Power Transmission, London, UK, March 2006.

[9] Nikolas Flourentzou, Vassilios G. Agelidis, and Georgios D. Demetriades, “ VSC-Based HVDC Power Transmission Systems: An Overview ”, IEEE Transactions on Power Electronics, Vol. 24, No. 3, March 2009.

[10] A. M. Abbas, and P. W. Lehn, “ PWM Based HVDC Systems- a Review ”, IEEE Power and Energy Society General Meeting, Calgary, AB Canada, 2009.

[11] Chang Hsin Chien, and Richard W. G. Bucknall, “ Analysis of Harmonics in Subsea Power Transmission Cables used in VSC-HVDC Transmisssion Systems Operating Under Steady-State Conditions ”, IEEE Transactions on Power Delivery, Vol. 22, No. 4, October 2007.

[12] Diego Valenza, and Gerri Cipollini, “ HVDC Submarine Power Cable Systems: State of the Art and Future Developments ”, International Conference on Energy Management and Power Delivery, Singapore, November 1995.

[13] Gunnar Asplund, “ Application of HVDC Light to Power System Enhancement ”, IEEE Power Engineering Society Winter Meeting, Singapore, January 2000.

[14] Björn Jacobson, Paulo Fischer de Toledo, Gunnar Asplund, and Marc Jeroense, “ City Infeed with HVDC LIGHT® and Extruded Cables ”, 16th

Conference on Electric Power Supply Industry, Mumbai, India, November 2006.

[15] Jiuping Pan, Reynaldo Nuqui, Kailash Srivastava, Tomas Jonsson, Per Holmberg, and Ying-Jiang Hafner, " AC Grid with Embedded VSC-HVDC for Secure and Efficient Power Delivery ", IEEE Energy 2030, Atlanta, GA USA November 2008.

[16] Guanjun Ding, Guangfu Tang, Zhiyuan He, and Ming Ding, " New Technologies of Voltage Source Converter (VSC) for HVDC Transmission System Based on VSC ", IEEE Power and Energy Society General Meeting-Conversion and Delivery of Electrical Energy in the 21st Century, Pittsburgh, PA USA, July 2008.

[17] S. Cole, D. Van Hertem, and R. Belmans, " VSC HVDC as an Alternative Grid Investment in Meshed Grids ", First International Conference on Infrastructure Systems and Services: Building Networks for a Brighter Future, Rotterdam, Netherlands, November 2008.

[18] Farhad Nozari, and Hasmukh S. Patel, " Power Electronics in Electric Utilities: HVDC Power Transmission Systems ", Proceedings of the IEEE, Volume 76, Issue 4, 1988.

[19] Frank Schettler, Hartmut Huang, and Norbert Christl, " HVDC Transmission Systems using Voltage Sourced Converters-Design and Applications ", IEEE Power Engineering Society Summer Meeting, Seattle, WA USA, July 2000.

[20] Lie Xu, and Vassilios G. Agelidis, " VSC Transmission System Using Flying Capacitor Multilevel Converters and Hybrid PWM Control ", IEEE Transactions on Power Delivery, Vol. 22, No. 1, January 2007.

[21] B. R. Andersen, L. Xu, and K. T. G. Wong, " Topologies for VSC Transmission ", 7th IEE International Conference on AC-DC Power Transmission, London, UK, November 2001.

[22] Jih-Sheng Lai, and Fang Zheng Peng, " Multilevel Converters-A new Breed of Power Converters ", IEEE Transactions on Industry Applications, Vol. 32, No. 3, May/June 1996.

[23] Guanjun Ding, Ming Ding, and Guangfu Tang, " An Innovative Hybrid PWM Technology for VSC in Application of VSC-HVDC Transmission System ", IEEE Electrical Power and Energy Conference, Vancouver, BC Canada, October 2008.

[24] Patrik Bujis, Stijn Cole, and Ronnie Belmans, " TEN-E Revisited: Opportunities for HVDC Technology ", 6th International Conference on the European Energy Market, Leuven, Belgium, May 2009.

[25] Cuiqing Du, Ambra Sannino, and Math H. J. Bollen, " Analysis of the Control Algorithms of Voltage-Source Converter HVDC ", IEEE Power Tech, St. Petersburg, Russia, June 2005.

[26] Temesgen M. Haileselassie, Marta Molinas, and Tore Undeland, " Multi-Terminal VSC-HVDC System for Integration of Offshore Wind Farms and Green Electrification of Platforms in the North Sea ", Nordic Workshop on Power and Industrial Electronics, Espoo, Finland, June 2008.

[27] Wang Yan, Zhao Shu-Zhen, Huangfu Cheng, and Ruan Jiang-Jun, " Dynamic Model and Control of Voltage Source Converter Based HVDC ", Asia-Pacific Power and Energy Engineering Conference, Wuhan, China, March 2009.

[28] Chengyong Zhao, and Chunyi Guo, " Complete-Independent Control Strategy of Active and Reactive Power for VSC Based HVDC System ", IEEE Power and Energy Society General Meeting, Calgary, AB Canada, July 2009.

[29] M. M. Zakaria Moustafa, and S. Filizadeh, " Electromagnetic Transient Simulation of a Back-to-Back Voltage Source Converter Based Transmission Scheme ", Canadian Conference on Electrical and Computer Engineering, Vancouver, BC Canada, April 2007.

[30] Guangkai Li, Gengyin Li, Haifeng Liang, and Chengyong Zhao, Ming Yin, " Research on Dynamic Characteristics of VSC-HVDC System ", IEEE Power Engineering Society General Meeting, Montreal, QC Canada, June 2006.

[31] Hairong Chen, " Research on the Control Strategy of VSC Based HVDC System Supplying Passive Network ", IEEE Power & Energy Society General Meeting, Calgary, AB Canada, July 2009.

[32] Mohamed M. Zakaria Moustafa, and S. Filizadeh, " Simulation of a VSC Transmission Scheme Supplying a Passive Load ", 34th Annual Conference of IEEE Industrial Electronics, Orlando, FL USA, November 2008.

[33] Gengyin Li, Ming Yin, Ming Zhou, and Chengyong Zhao, " Modeling of VSC-HVDC and Control Strategies for Supplying both Active and Passive

Systems ”, IEEE Power Engineering Society General Meeting, Montreal, QC Canada, June 2006.

[34] Guibin Zhang, Zheng Xu, and Hongtao Liu, “ Supply Passive Networks with VSC-HVDC ”, IEEE Power Engineering Society Summer Meeting, Vancouver, BC Canada, July 2001.

[35] Y. Iwata, S. Tanaka, K. Sakamato, H. Konishi, and H. Kawazoe, “ Simulation Study of a Hybrid HVDC System Composed of a Self Commutated Converter and a Line Commutated Converter ”, 6th IEE International Conference on AC and DC Power Transmission, London, UK, May 1996.

[36] Z. Zhao, and M.R. Iravani, “ Application of a GTO Voltage Source Inverter in a Hybrid HVDC Link ”, IEEE Transactions on Power Delivery, Vol. 9, No. 1, January 1994.

[37] Guangkai Li, Gengyin Li, Haifeng Liang, Ming Yin, and Chengyong Zhao, “ Operational Mechanism and Characteristic Analysis of Novel Hybrid HVDC System ”, International Conference on Power System Technology, Chongqing, China, October 2006.

[38] Guangkai Li, Gengyin Li, Haifeng Liang, Chengyong Zhao, and Ming Yin, “ Research on Hybrid HVDC ”, International Conference on Power System Technology, Singapore, November 2004.

[39] Willis Long, and Stig Nilsson,“ HVDC Transmission: Yesterday and Today ”, IEEE Power and Energy Magazine, March/April 2007.

[40] R. Rudervall, and J. P. Charpentier, and R. Sharma, " High voltage direct current (HVDC) transmission systems technology review paper ", in Energy Week 2000, March 2000.

[41] Owen Peake, " The History of High Voltage Direct Current Transmission ", 3rd Australian Engineering Heritage Conference, Dunedin, New Zealand, November 2009.

[42] Dennis A. Woodford, " HVDC transmission ", Manitoba HVDC Research Centre, Tech. Rep., 1998.

[43] Chan-Ki Kim, Vijay K. Sood, Gil-Soo Jang, Seong-Joo Lim, and Seok-Jin Lee, " HVDC Transmission: Power Conversion Applications in Power Systems ", John Wiley & Sons, ISBN 978-0-470-82295-1, 2009.

[44] M. P. Bahrman, J.G. Johansson, and B.A. Nilsson, " Voltage source converter transmission technologies: the right fit for the application ", IEEE Power Engineering Society General meeting, Toronto, ON Canada, July 2003.

[45] Paulo Fischer de Toledo, " Feasibility of HVDC for City Centre Infeed ", Licentiate Thesis, Royal Institute of Technology, Sweden, 2003.

[46] http://www.EMTP-RV.com/

[47] Jos Arrillaga, Y. H. Liu, N. R. Watson, " Flexible Power Transmission: The HVDC Options ", ISBN 978-0-470-05688-2, 2009.

# Appendix A

## Load Impedance Calculations

The inverter load at the receiving end network was rated at 2.4 MVA, which is equivalent to 80% of the inverter rating. The load is fed at 33 kV with a power factor (pf) of 0.8 lagging.

In order to determine the load impedance, the load current was calculated using the above load data.

The full load current is calculated by equation (A.1):

$$I_{full\ load} = \frac{S_{full\ load}}{\sqrt{3} \times V_{load}} \tag{A.1}$$

$$I_{full\ load} = 42\ A \tag{A.2}$$

The active and reactive power of the load are found by equations A.3 and A.5:

$$P_{full\ load} = S_{full\ load} \times pf \tag{A.3}$$

$$P_{full\ load} = 1.92\ MW \tag{A.4}$$

$$Q_{full\ load} = S_{full\ load} \times \sin(\cos^{-1}(pf)) \tag{A.5}$$

$$Q_{full\ load} = 1.44\ MW \tag{A.6}$$

From A1.2 and A1.4 and assuming a balanced 3-phase load, the resistive part of the load impedance is calculated using A1.7 as follows:

$$P_{full\ load} = I^2_{full\ load} \times R_{full\ load} \tag{A.7}$$

$$R_{full\ load} = 363\ \Omega \tag{A.8}$$

Similarly, the inductive part of the load impedance is calculated using A.9 from A.2 and A.6 as follows:

$$Q_{full\ load} = I^2_{full\ load} \times X_{full\ load} \quad \text{(A.9)}$$

$$X_{full\ load} = 272\ \Omega \quad \text{(A.10)}$$

$$L_{full\ load} = 0.72\ H \quad \text{(A.11)}$$

Assuming that the load is split into $n$ switchable branches of equal impedances, the branch impedance is calculated using A.12 as follows:

$$Z_{branch} = \frac{Z_{full\ load}}{n} \quad \text{(A.12)}$$

Substituting $n = 10$ in A.12, the resistive and inductive parts of branch impedance are given by A.13 and A.14 as follows:

$$R_{branch} = 3630\ \Omega \quad \text{(A.13)}$$

$$X_{branch} = 7.22\ H \quad \text{(A.14)}$$

# Appendix B

## Harmonic Filters Calculations

Harmonic filters were used at rectifier and inverter terminals in order to remove the dominant harmonics in bus voltage. The following is the Matlab M-code that was used to calculate the values of resistance, inductance, and capacitance for each tuned harmonic filter.

```
% Low pass filter design program
% Filter connection is wye
% Fundamental frequency =  60 Hz
Q=input('Please enter the filter rating (MVA)');
V=input('Please enter the system voltage (kV line to line)');
n=input('Please enter the harmonic order');
quality=input('Please enter the quality factor');
f=60;
omega=2*pi*f;
C=Q/(omega*(V^2))
L=1/(C*(n*omega)^2)
R=(omega*L)/quality
```

The following is the Matlab M-code that was used to calculate the values of resistance, inductance, and capacitance for the high pass damped filter used at the inverter terminal.

```
% High Pass (HP) Damped Filter design program
% Filter connection is wye
% frequency = 60 Hz
Q=input('Please enter the filter rating (MVA)');
V=input('Please enter the system voltage (kV line to line)');
n=input('Please enter the harmonic order');
quality=input('Please enter the quality factor');
f=60;
omega=2*pi*f;
C=Q/(omega*(V^2))
L=1/(C*(n*omega)^2)
R=quality*omega*L
```